# Dominant Factors Influencing the Seasonal Predictability of U.S. Precipitation and Surface Air Temperature

R. W. HIGGINS, A. LEETMAA, Y. XUE, AND A. BARNSTON

*Climate Prediction Center, NOAA/NWS/NCEP, Washington, D.C.*

(Manuscript received 30 June 1999, in final form 8 February 2000)

ABSTRACT

The relative contributions of El Niño–Southern Oscillation (ENSO), long-term tropical Pacific variations, and the Arctic oscillation (AO) to the explained variance of U.S. precipitation and surface air temperature are investigated. The time variability of monthly precipitation in the tropical Pacific basin is separated into high-pass and low-pass filtered components. The leading EOFs of the high-pass and low-pass filtered data capture ENSO cycle–related interannual variability and ENSO-like interdecadal variability, respectively. The dominant mode of variability in the extratropics is the AO, which has been implicated in some of the secular variability of climate in the Northern Hemisphere extratropics.

ENSO produces large, reasonably reproducible spatial and temporal shifts in tropical precipitation. The tropical interdecadal variability produces more subtle, but still significant, shifts in tropical precipitation that contribute significantly to the explained variance and to trends in the North Pacific sector, over the United States, and extending into the North Atlantic sector. Consistent with previous studies, the largest and most significant AO-related contributions are during the cold season (October–March), particularly over the eastern half of the United States, the North Atlantic sector, Eurasia, and the polar cap.

The results indicate that a significant portion of the skill of climate forecast models will likely arise from an ability to forecast the temporal and spatial variability of the interdecadal shifts in tropical precipitation as well as the associated teleconnection patterns into midlatitudes. Because the AO encompasses the North Atlantic oscillation, it appears that additional increases in skill over portions of North America require forecasts of the AO.

## 1. Introduction

Like most regions of the globe, the United States experiences climate variations on timescales ranging from intraseasonal to decadal. The challenge facing the climate community is to develop and implement a capability to forecast these variations. In recent years the reanalyses produced by the operational centers [e.g., the National Centers for Environmental Prediction–National Center for Atmospheric Research (NCEP–NCAR reanalysis (Kalnay et al. 1996) and the European Centre for Medium-Range Weather Forecasts reanalysis (Gibson et al. 1997)] have played a critical role in this. In addition to providing core datasets for initial conditions in climate forecast systems, the reanalyses are instrumental for diagnostic studies of the physical origins of climate variability.

One might anticipate that the skill of any climate forecast system would be determined by the presence of the dominant modes of the coupled atmosphere–ocean system. The best known of these modes is the El Niño–Southern Oscillation (ENSO) phenomenon (e.g., Rasmusson and Carpenter 1982). In operational seasonal precipitation and temperature forecasts extensive use is made of the fact that El Niños and La Niñas tend to have repeatable influences on U.S. weather.

At present, several atmospheric general circulation models are capable of reproducing the average response of the atmosphere to changes in tropical Pacific sea surface temperatures (SSTs) associated with ENSO. However, the model responses are too reproducible, look more like each other than the observations, and exhibit too much antisymmetry (i.e., equal but opposite) between the El Niño and La Niña influences. Clearly, getting the models to respond correctly to typical ENSO SST anomalies and to less typical SST distributions (e.g., interdecadal shifts) is critical to extending predictability for seasonal to interannual variability.

Anomalous shifts in tropical convection on decadal timescales are also important in producing U.S. and global climate variability. A zero-order way to describe these longer-term variations is to fit linear trends to describe circulation changes or changes in precipitation and temperature regimes and distributions. One can then

*Corresponding author address:* Dr. R. W. Higgins, Analysis Branch, Climate Prediction Center, NOAA/NWS/NCEP, World Weather Building, 5200 Auth Road, Camp Springs, MD 20746-4304. E-mail: whiggins@ncep.noaa.gov

TABLE 1. Datasets used in this study.

| Field | Resolution | Period of record | Source |
|---|---|---|---|
| Precipitation | 2.5 × 2 | 1948–96 | NCDC hourly precipitation data (Higgins et al. 1996) |
| Surface air temperature | 0.5 × 0.5 | 1948–93 | NCDC daily cooperative data (Janowiak and Bell 1998) |
| Geopotential height and winds | 2.5 × 2.5 | 1948–98 | NCEP–NCAR reanalysis (Kalnay et al. 1996) |
| Sea surface temperature | 2.0 × 2.0 | 1950–98 | Climate Prediction Center (Reynolds and Smith 1995; Smith et al. 1996) |
| Pacific basin precipitation (66 sites) | — | 1955–96 | Climate Predicition Center (He et al. 1998) |
| CPC merged analysis of precipitation | 2.5 × 2.5 | 1979–98 | Climate Prediction Center (Xie and Arkin 1996, 1998) |

search for the dominant modes of climate variability, in addition to ENSO, that contribute to these trends.

The utility of knowing what type of decadal climate regime is operative has been well demonstrated in previous studies (e.g., Douglas et al. 1982). Given this knowledge, the idea is that seasonal forecasts can be improved upon by incorporating decadal trends into the forecast. The use of decadal trends in seasonal forecasting is currently employed by the Climate Prediction Center (CPC). Using rotated canonical correlation analysis between U.S. surface temperature and global SST, Livezey and Smith (1999) identified two signals with considerable variance on interdecadal or longer timescales. They showed that the associated upper-air circulation patterns have significant projections on the Pacific–North America pattern (PNA) and the North Atlantic oscillation (NAO).

In this study we propose a climate signal separation that builds on previous work to examine the seasonal predictability of U.S. precipitation and surface air temperature. The time variability of monthly precipitation in the tropical Pacific basin is separated into high-pass and low-pass filtered components. The leading EOFs of the high-pass and low-pass filtered data capture ENSO

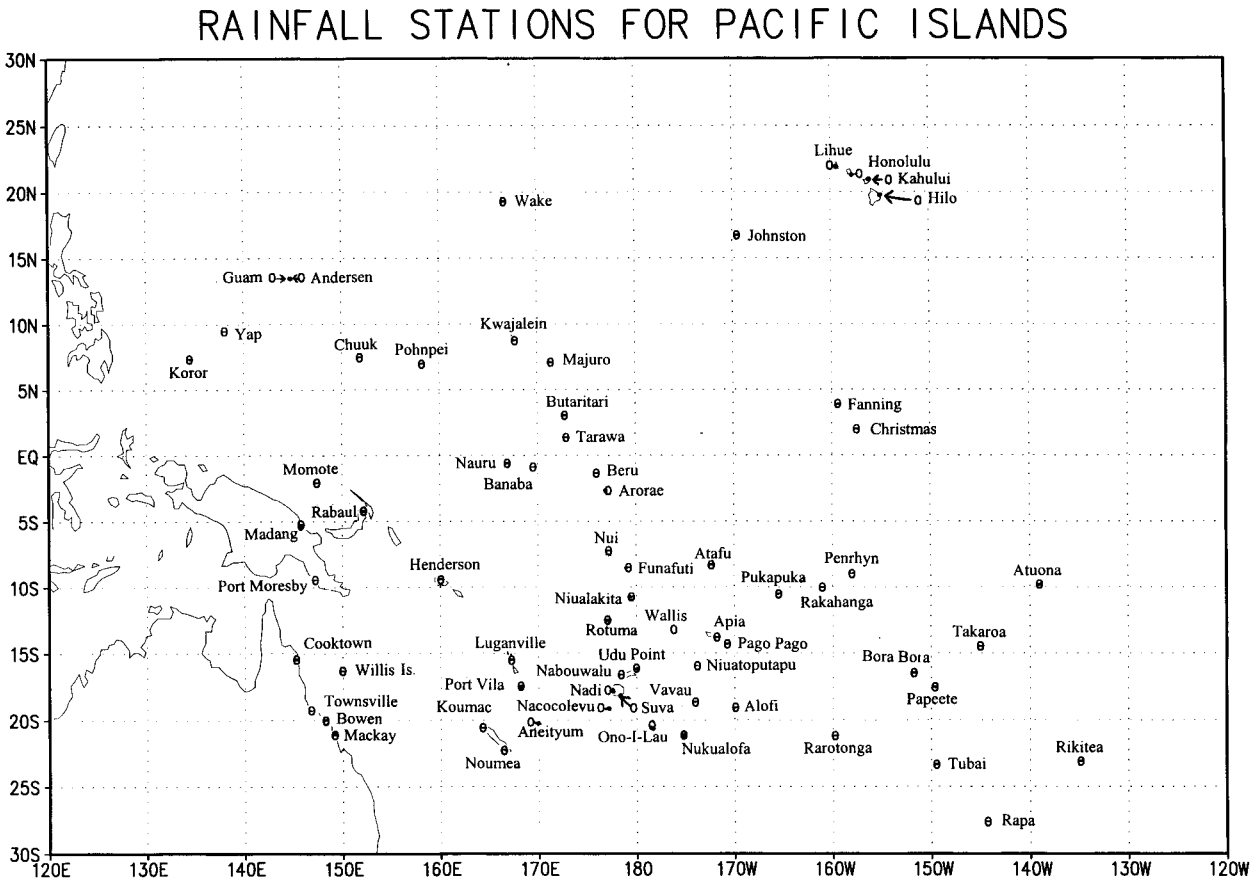


FIG. 1. Locations of the 66 Pacific basin stations analyzed here and in the Atlas of He et al. (1997).

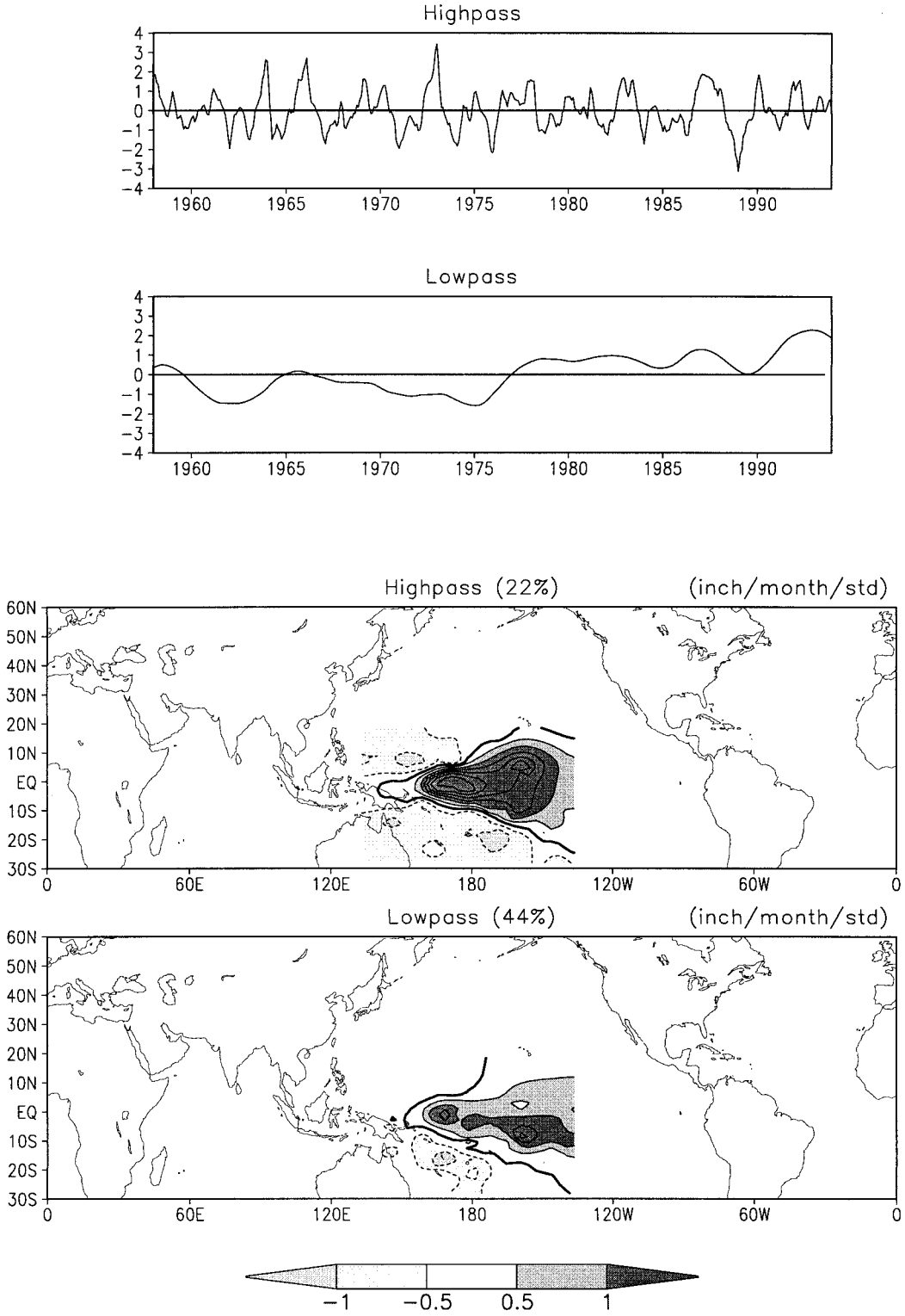


FIG. 2. The leading (normalized) principal component (PC) time series of 7-yr-HP- and LP-filtered Pacific basin precipitation together with the associated spatial patterns. The interval between tick marks on the vertical axis of the top panel corresponds to 1.0 std dev. The leading PCs are shown for all months of the year. Contour interval is 0.5 in. (std dev)$^{-1}$ of the expansion coefficient time series. Negative contours are dashed and the zero contour is thickened. Positive (negative) values greater than 0.5 in. (std dev)$^{-1}$ [less than $-0.5$ in. (std dev)$^{-1}$] are shaded dark (light).

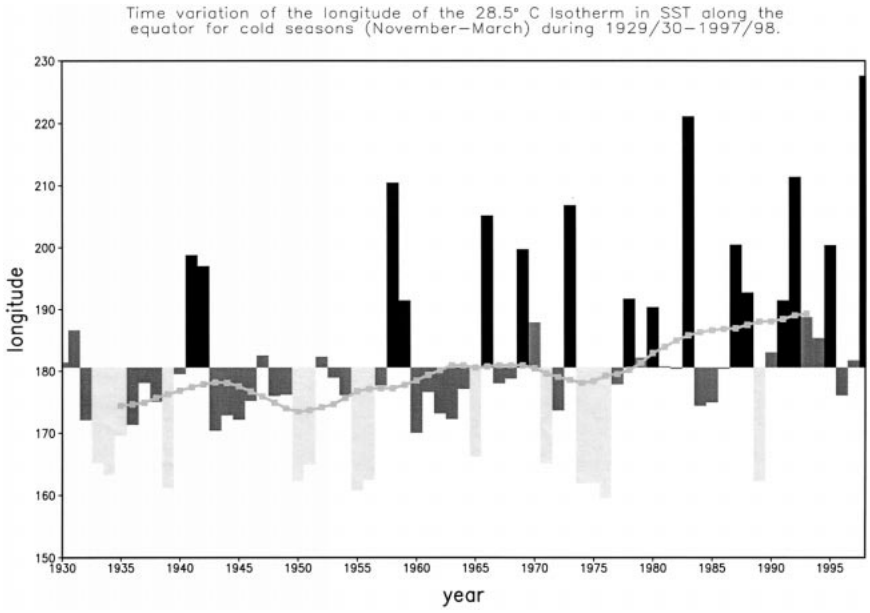


FIG. 3. Time variation of the longitude of the 28.5°C isotherm in SST along the equator (4°N–4°S) for cold seasons (Oct–Mar) from 1929–30 to 1997–98. The mean longitude for the period is 179.4°W. Ten-year running mean values are indicated by the line with closed squares. Warm (cold) ENSO episodes are indicated by the dark (light) shading, while neutral episodes are indicated by the medium shading.

cycle-related interannual variability and ENSO-like interdecadal variability, respectively. This approach is similar to that used by Zhang et al. (1997), but here we use tropical precipitation rather than SST. Our rationale for this is the more direct physical linkage between fluctuations in the atmospheric circulation and fluctuations in tropical precipitation. The dominant mode of variability in the extratropics is the Arctic oscillation (hereafter AO), which Thompson and Wallace (1998, 2000) have shown to be the primary mode of wintertime variability over the Northern Hemisphere (NH) extratropics on timescales ranging from intraseasonal to interdecadal. The AO incorporates many of the features of the associated, more localized NAO (e.g., Hurrell 1995; Hurrell and van Loon 1997) but its larger horizontal scale and higher degree of zonal symmetry render it more like a surface signature of the polar vortex aloft. Thompson and Wallace (1998) showed that the AO accounts for a substantially larger fraction of the variance of NH surface air temperature than the NAO.

This climate decomposition is used to show that decadal shifts in tropical precipitation account for a sizable fraction of the total variance and observed trends in the Pacific sector and over the United States. It is argued that a significant portion of the skill of climate forecast models, in addition to that already harvested from ENSO variability, will arise from an ability to forecast the temporal and spatial variability of these shifts as well as the associated teleconnection patterns into midlatitudes. The results highlight the need for modeling experiments aimed at simulating the more subtle decade-scale SST variability in the western Pacific and Indian Ocean and the associated shifts in tropical precipitation. Because the AO encompasses the NAO, it appears that additional increases in skill will require forecasts of the AO.

The datasets and analysis procedures used in this study are discussed in section 2. Appropriate indices representing tropical interannual, tropical interdecadal, and extratropical variability are introduced in section 3. These indices are used to investigate the seasonal predictability of the NH circulation and U.S. precipitation and surface air temperature in section 4. Recent trends in the same fields are discussed in section 5. A summary and discussion are given in section 6.

## 2. Datasets and analysis procedures

Several monthly mean gridded datasets are used in this study: U.S. precipitation extracted from the National Climatic Data Center (NCDC) Hourly Precipitation Data (Higgins et al. 1996), U.S. surface air temperature extracted from the NCDC ''Cooperative Summary of the Day'' (Janowiak et al. 1999), geopotential height and winds from the NCEP–NCAR reanalysis (Kalnay et al. 1996), sea surface temperature from the historical reconstruction of Smith et al. (1996), and the CPC merged analysis of precipitation (Xie and Arkin 1996, 1998). The periods of record and resolution of the gridded datasets are indicated in Table 1.

In section 3a we present an EOF analysis based on monthly precipitation data from 66 stations in the trop-

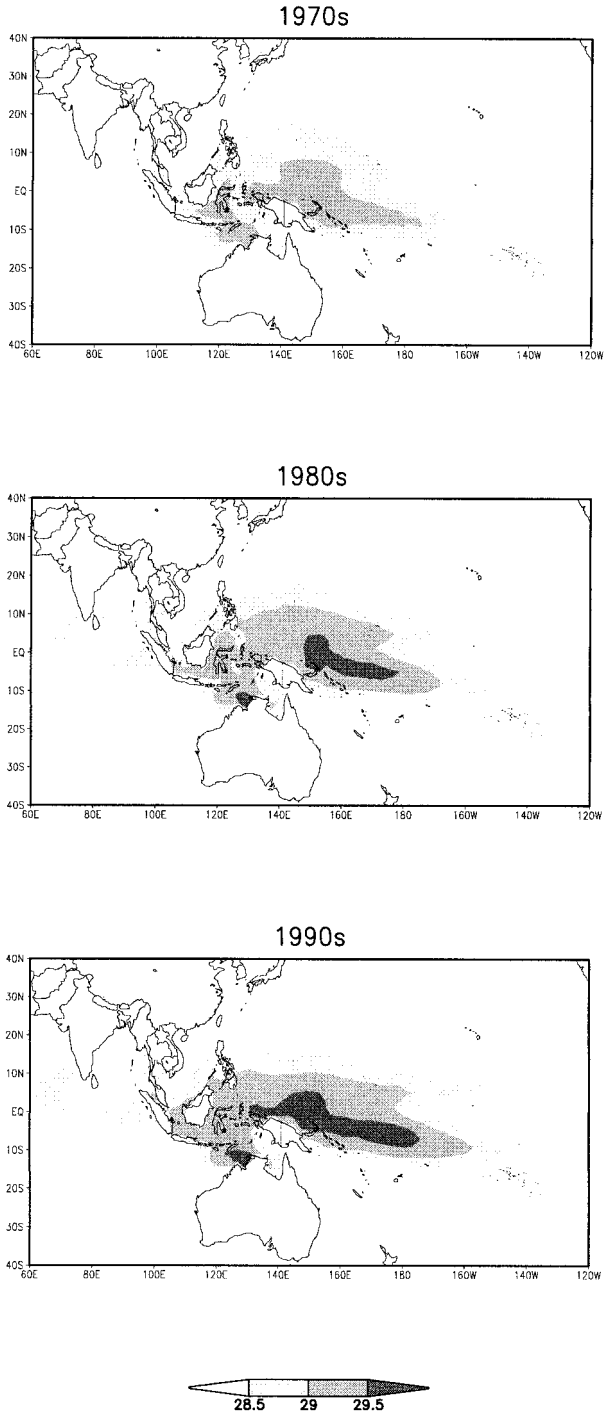


FIG. 4. Size of the west Pacific warm pool as measured by the area with SSTs at or above 28.5°, 29°, and 29.5°C during the 1970s, 1980s, and 1990s. The averages are for the NH cold season (Oct–Mar).

ical Pacific basin (He et al. 1998) for the period 1955–96; the stations are shown in Fig. 1. Prior to the EOF analysis, the annual cycle is removed from each station individually. Low-pass filtered time series are generated by application of a 7-yr running mean to the monthly anomalies for each station. Corresponding 7-yr high-pass filtered time series are formed by subtracting the 7-yr low-pass filtered time series from the original time series (without tapering). The leading EOFs of the high-pass and low-pass filtered data capture ENSO cycle-related interannual variability and ENSO-like interdecadal variability, respectively. The EOF analysis is based on the covariance matrix. In sections 4 and 5 seasonal mean time series are used, where winter, spring, summer, and autumn are defined as January–March (JFM), April–June (AMJ), July–September (JAS), and October–December (OND), respectively.

Regression maps in section 3 are formed by regressing gridpoint values of the appropriate field upon the normalized principal component (PC) time series. The contours on these maps have the same dimensions as the fields themselves, and their numerical values are indicative of the anomalies associated with typical (i.e., unit standard deviation) amplitudes.

In section 4 we establish temporal correlation skill benchmarks of seasonal simulations using a linear empirical model (simple linear regression) that exploits our climate decomposition. Benchmarks are established using a cross-validated version of the linear correlation between the observed and simulated fields (SST, 200-hPa eddy streamfunction, and U.S. precipitation and surface air temperature). In cross validation, the data for the years being simulated are held out of the regression, such that only the remaining years are used to define the climatology (mean and standard deviation) and the linear regression equation. Because a 7-yr running mean is applied to obtain the high-pass (HP) and low-pass (LP) indices, we withold 7 consecutive years from the regression for each forecast. Only the one year at the center of each 7-yr period is simulated as an independent case. Each 7-yr period is held out this way in turn, and a temporal correlation skill is computed from the corresponding simulations and observations (each normalized with respect to the standard deviation of the appropriate training period). The cross-validated skill is slightly lower than the correlation between the observed and predicted variable using all years. Skills are adjusted for a degeneracy that occurs in cross validation with regression (Barnston and van den Dool 1993) using the approach discussed in Peng et al. (2000).

In section 5 we estimate the relative contributions of ENSO-like interdecadal variability and the AO to recent trends in the NH circulation and in United States precipitation and surface air temperature. Contributions to the total trends are estimated using the methodology of Thompson et al. (2000). Total linear trends are estimated as the slope of a straight line fitted (in a least squares sense) to the observed data at each grid point. Contributions to these linear trends are estimated at each grid point by regressing seasonal values of a grid point's time series onto the appropriate index (indices are defined in section 3), and then by multiplying the resulting regression coefficient by the linear trend in the index.

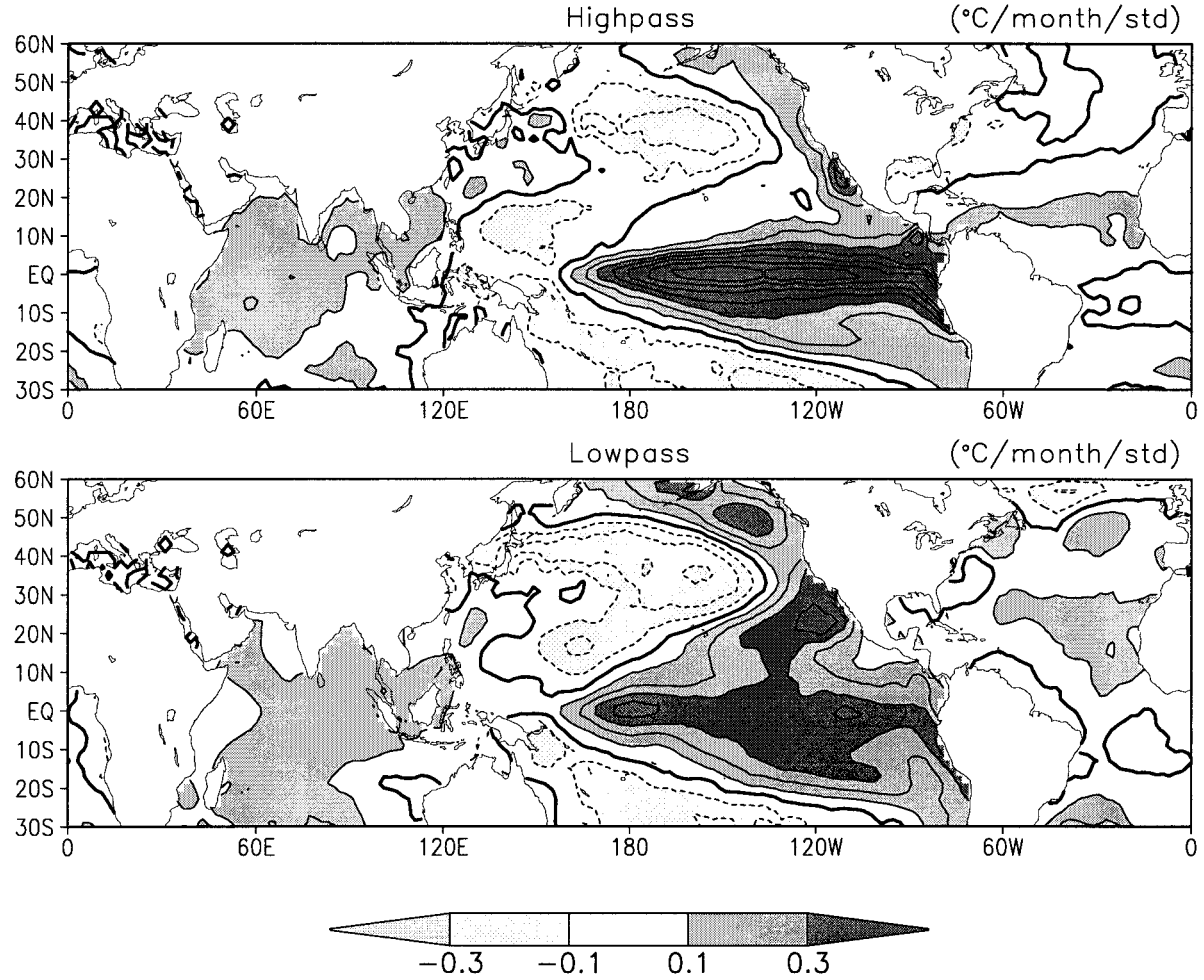


FIG. 5. Spatial patterns generated by regressing the global SST field upon the HP and LP indices shown in the top panels of Fig. 2. Contour interval is 0.1°C (std dev)$^{-1}$ of the expansion coefficient time series. Negative contours are dashed; the zero contour is thickened. Positive (negative) values greater than 0.1°C (less than −0.1°C) are shaded dark (light).

## 3. Tropical and extratropical variability

### *a. Tropics*

The leading (normalized) PC time series of 7-yr high-pass and low-pass filtered Pacific basin precipitation, labeled as HP and LP, respectively, together with the associated spatial patterns are shown in Fig. 2; hereafter we refer to the time series as the HP index and the LP index, respectively. The HP index captures most of the variability associated with the ENSO cycle. This time series is strongly correlated with the Niño-3.4 SST index ($r = 0.76$, where $r$ denotes the correlation coefficient), with SST appearing to lead precipitation slightly. Due to spatial gaps in the tropical precipitation station network, ENSO events that are concentrated in the eastern portion of the Pacific basin (such as the 1982–83 event) are somewhat underestimated by the HP index.

The LP index captures the break around 1976–77 (as was the case for the SST-based LP index in Zhang et al. 1997). Other differences between the time series imply that LP-related contributions to seasonal predictability (section 4) and trends (section 5) will be different depending on whether precipitation or SST is used. Loadings in the spatial pattern are oriented from west-northwest to east-southeast in the vicinity of the South Pacific convergence zone. The LP index is related to the gradual eastward expansion of the warm pool in the western Pacific that has been occurring since at least the 1950s (Figs. 3 and 4). In fact, when a monthly warm pool index is constructed by averaging SSTs over the area 6°N–6°S, 120°E–170°W, we find that it correlates significantly with the monthly LP index ($r = 0.60$) and with a monthly global surface temperature index ($r = 0.66$) produced by the CPC (Ropelewski et al. 1985). This is an indication that the expansion of the warm pool and the associated interdecadal shifts in tropical convection cannot be ruled out as manifestations of global climate change. The

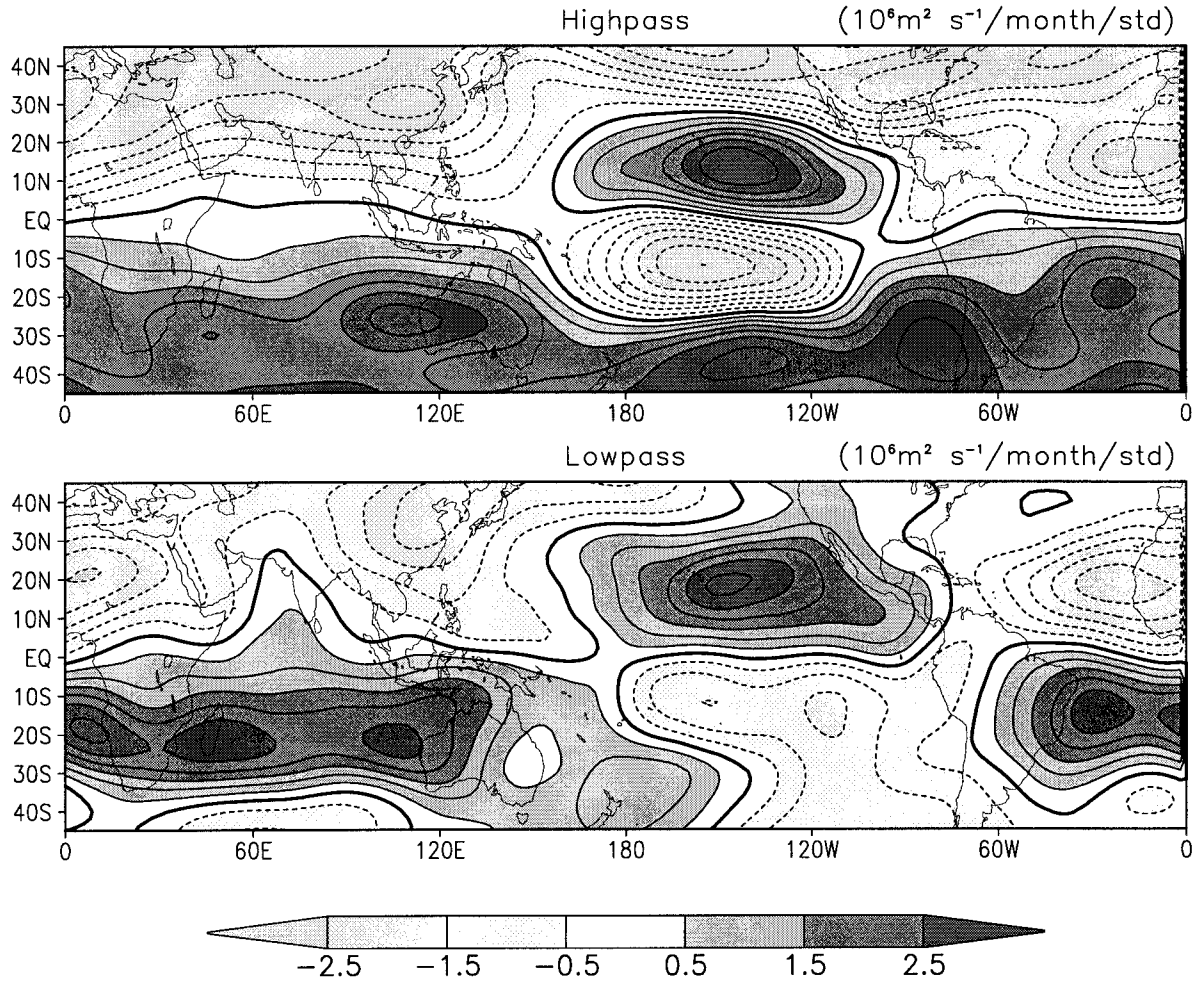


FIG. 6. Spatial patterns generated by regressing the global 200-hPa streamfunction field upon the HP and LP indices shown in the top panels of Fig. 2. Contour interval is $0.5 \times 10^6$ m$^2$ s$^{-1}$ (std dev)$^{-1}$ of the expansion coefficient time series. Negative contours are dashed and the zero contour is thickened. Positive (negative) values greater than $0.5 \times 10^6$ m$^2$ s$^{-1}$ (less than $-0.5 \times 10^6$ m$^2$ s$^{-1}$) are shaded dark (light).

monthly LP and HP indices are negligibly correlated ($r = 0.12$), suggesting that we have a reasonably good separation of the tropical interannual and interdecadal variability.

The spatial signatures obtained by regressing the global SST field upon the HP and LP indices (Fig. 5) are similar to those shown in Zhang et al. (1997) (see their Fig. 3). The two patterns in Fig. 5 are qualitatively similar, with large SST anomalies in the tropical Pacific, anomalies of opposite polarity in the equatorial central North Pacific, and a high degree of equatorial symmetry. The equatorial maximum in the eastern Pacific is more pronounced and more narrowly confined along the equator in the HP, whereas the SST fluctuations in the extratropical central North Pacific are more prominent in the LP. In section 4 we will show that the 200-hPa streamfunction field more closely resembles the PNA pattern in regressions involving the LP index than the HP index (the same is true for the 500-hPa field). In addition to Zhang et al. (1997), other investigators, including Wang (1995) and Yukimoto et al. (1996), have obtained similar patterns using different filtering approaches. Because the interdecadal variability exhibits a spatial signature that is similar in many respects to ENSO, it is difficult to compare these results with studies that have attempted to recover separate ''modes'' of variability (e.g., Parker and Folland 1991; Deser and Blackmon 1995; Latif et al. 1997). In view of this, and the limited length of the historical record, we will not formally refer to the interdecadal variability as a separate mode (e.g., such as the Pacific decadal oscillation). We note that a regression of global SST onto the North Pacific SST index of Latif and Barnett (1996) produces a pattern quite similar to that shown in Fig. 5b, except that there is relatively more loading in the North Pacific sector. The correlation between monthly values of the LP and North Pacific SST indices ($r = -0.53$) is significant at the 95% level after accounting for the reduced

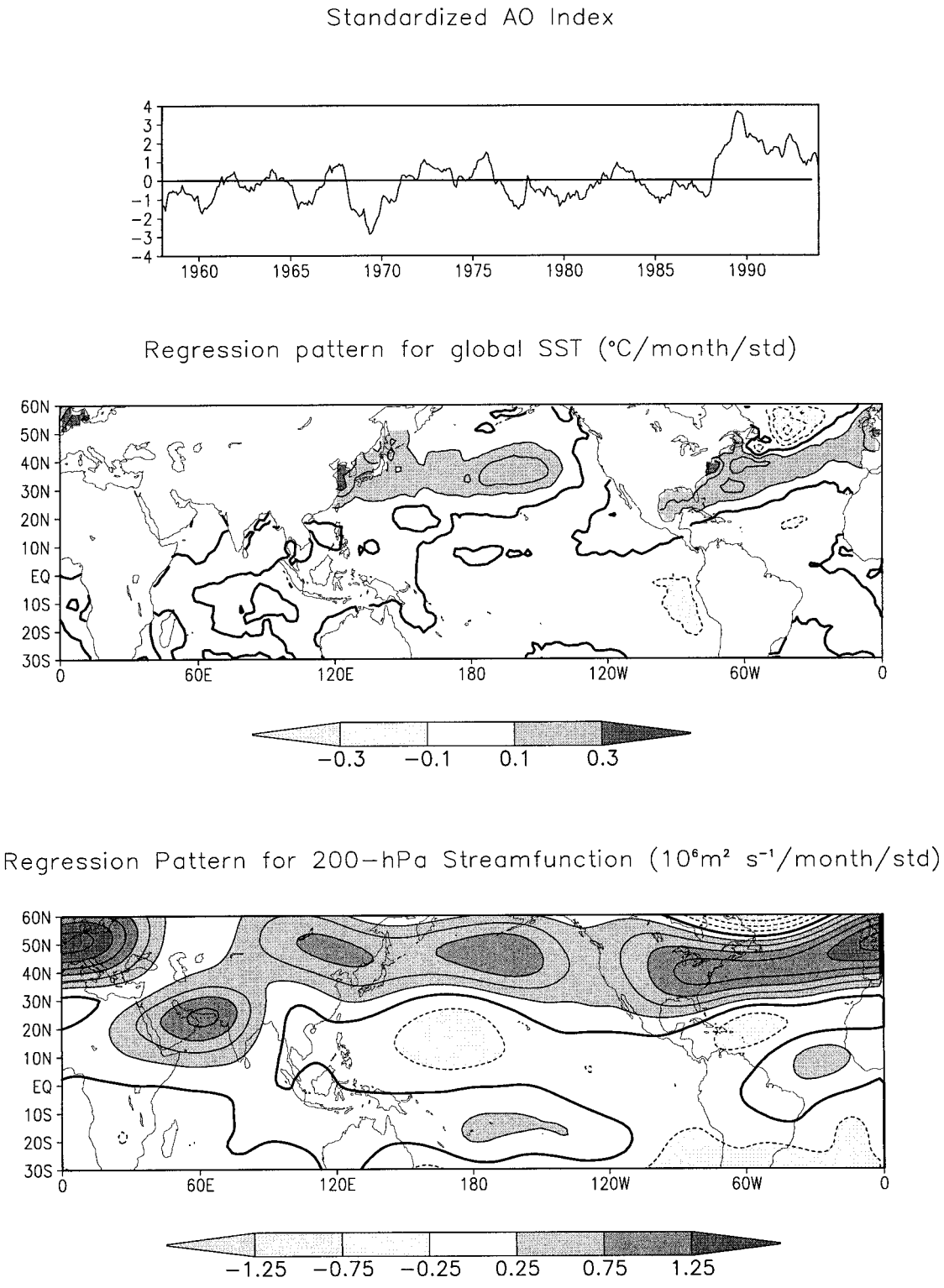


FIG. 7. The AO index (Thompson and Wallace 1998) together with the associated regression pattern for global SST and 200-hPa streamfunction. The AO index is shown for all months of the year. Contour intervals are 0.1°C and $0.5 \times 10^6$ m$^2$ s$^{-1}$ (std dev)$^{-1}$ of the expansion coefficient time series, respectively. Negative contours are dashed and the zero contour is thickened.

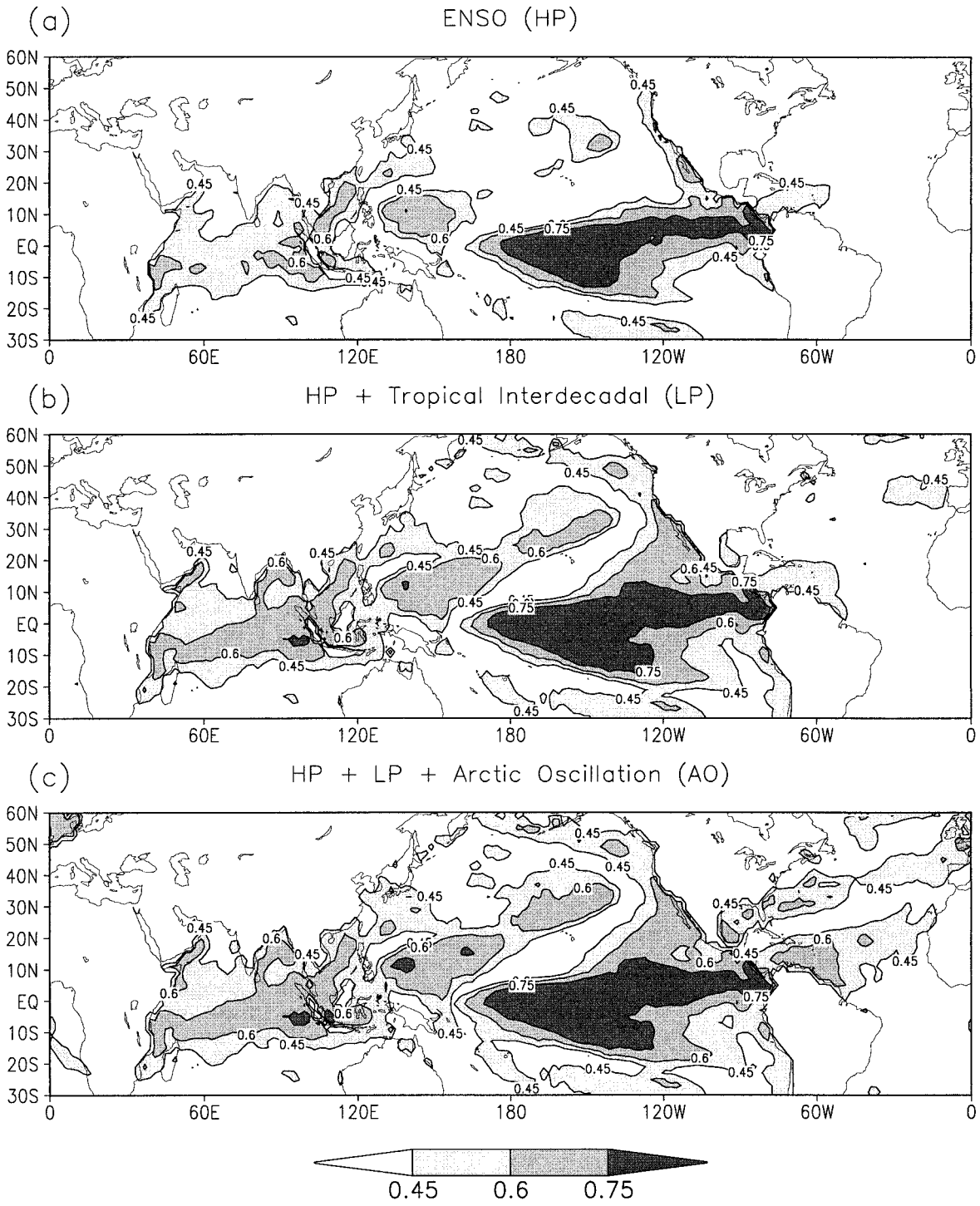


FIG. 8. The 36-yr (1958–93) correlation between time series of JFM observed and reconstructed SST. The reconstructed time series are obtained by regressing the observed SST onto (a) the HP index, (b) the HP and LP indices, and (c) the HP, LP, and AO indices. The critical value of the correlation coefficient (significant at the 95% level) is 0.32.

effective sample size brought about by the integral timescale of more than 1 yr.

The spatial signatures obtained by regressing monthly global 200-hPa streamfunction anomalies upon the HP and LP indices are shown in Fig. 6. The HP pattern shows twin anticyclones on either side of the equator in the central tropical Pacific, ringed by cyclonic circulation centers in the midlatitudes of both hemispheres.

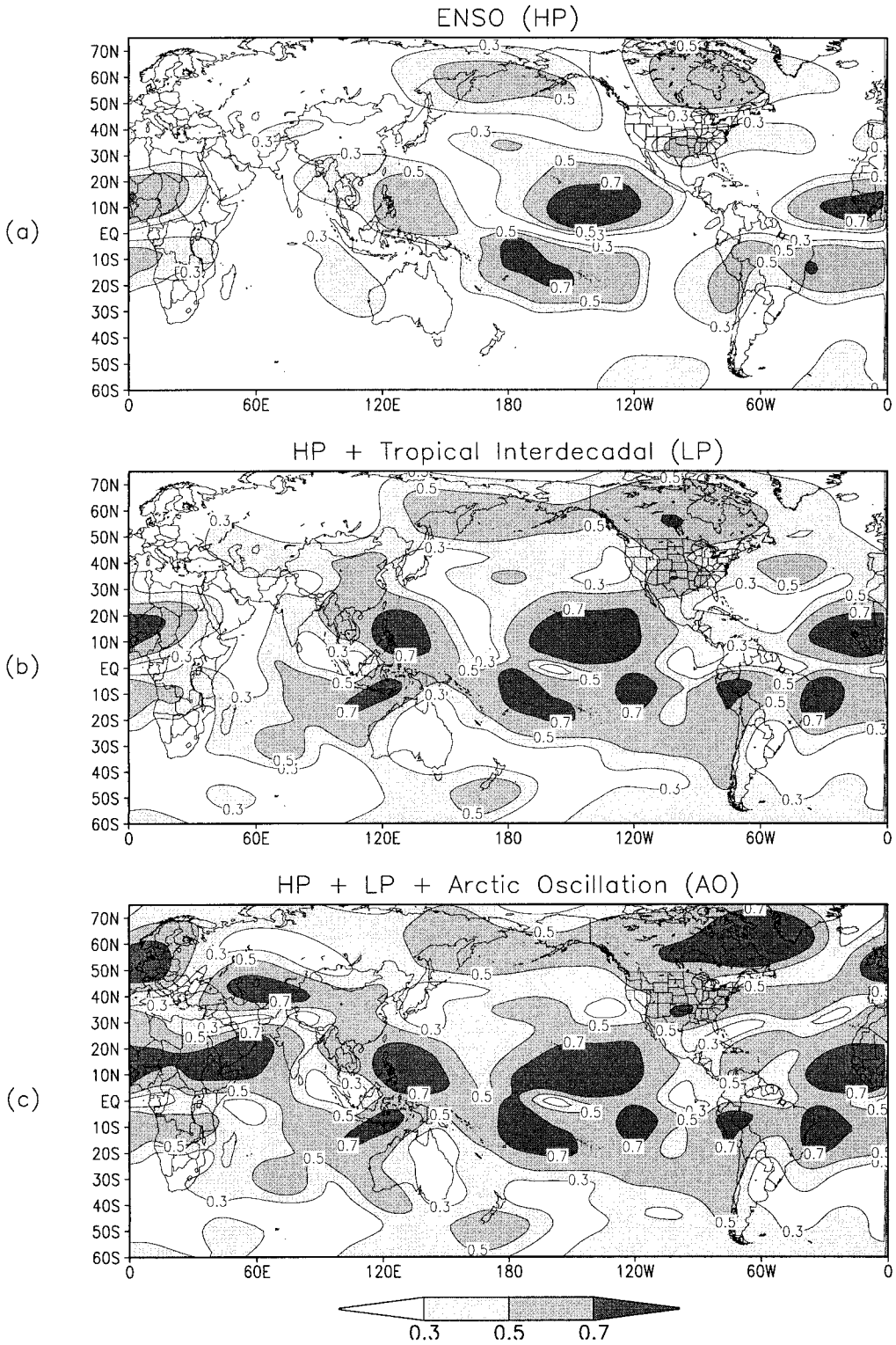


FIG. 9. The 36-yr (1958–93) correlation between time series of JFM observed and reconstructed 200-hPa streamfunction. The reconstructed time series are obtained by regressing the 200-hPa streamfunction onto (a) the HP index, (b) the HP and LP indices, and (c) the HP, LP, and AO indices. The critical value of the correlation coefficient (significant at the 95% level) is 0.32.

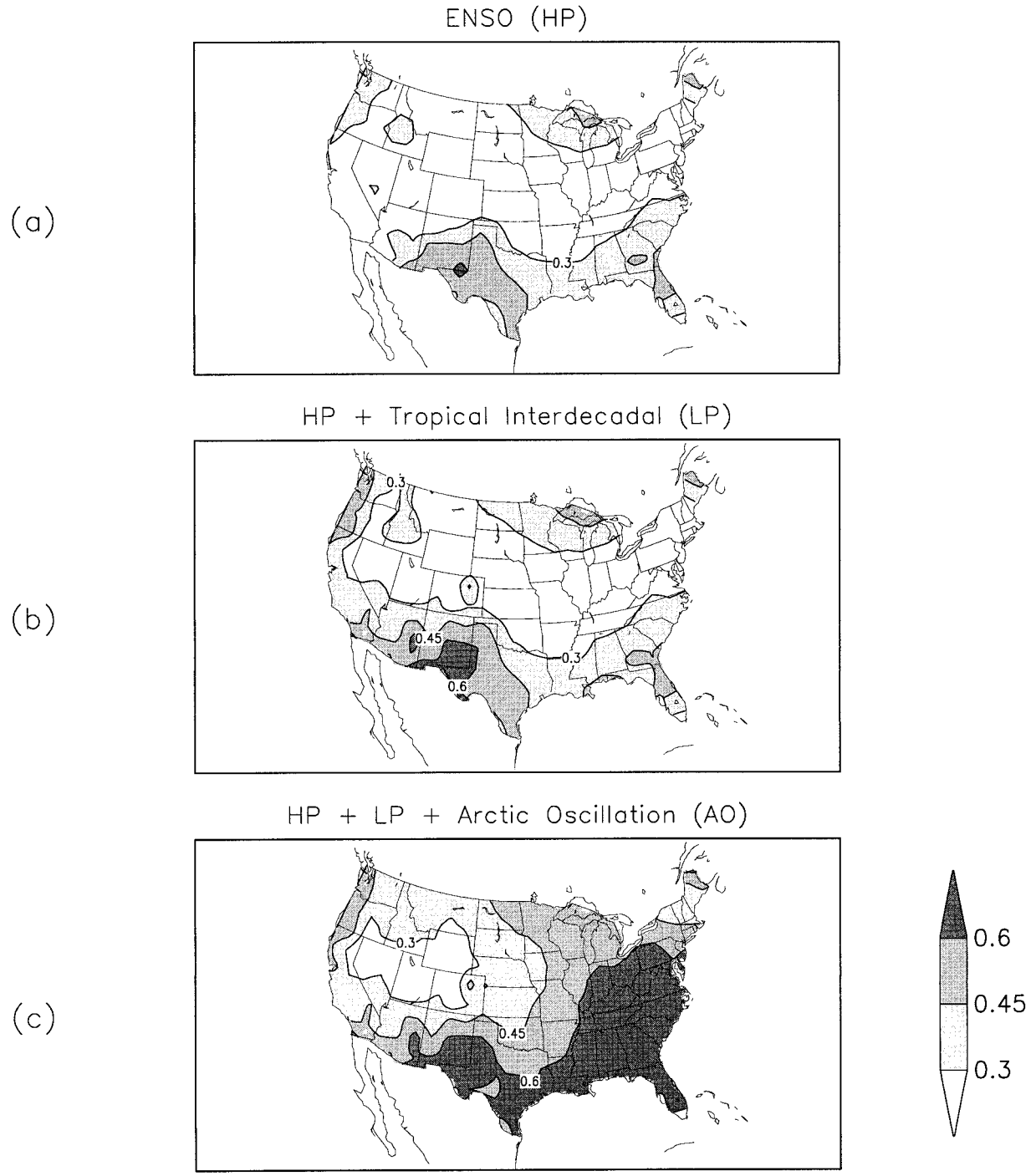


FIG. 10. The 36-yr (1958–93) correlation between time series of JFM observed and JFM reconstructed U.S. surface air temperature. The reconstructed time series are obtained by regressing the observed surface air temperature onto (a) the HP index, (b) the HP and LP indices, and (c) the HP, LP, and AO indices. The critical value of the correlation coefficient (significant at the 95% level) is 0.32.

In general, the LP pattern is qualitatively similar, except over North America and portions of the eastern South Pacific. Recall that the LP index changes sign in the mid-1970s (Fig. 2), which implies a flip in the LP spatial pattern (Fig. 6, lower panel).

### *b. Extratropics*

Thompson and Wallace (1998, 2000) showed that the leading modes of variability of the extratropical circulation in both hemispheres are characterized by deep,

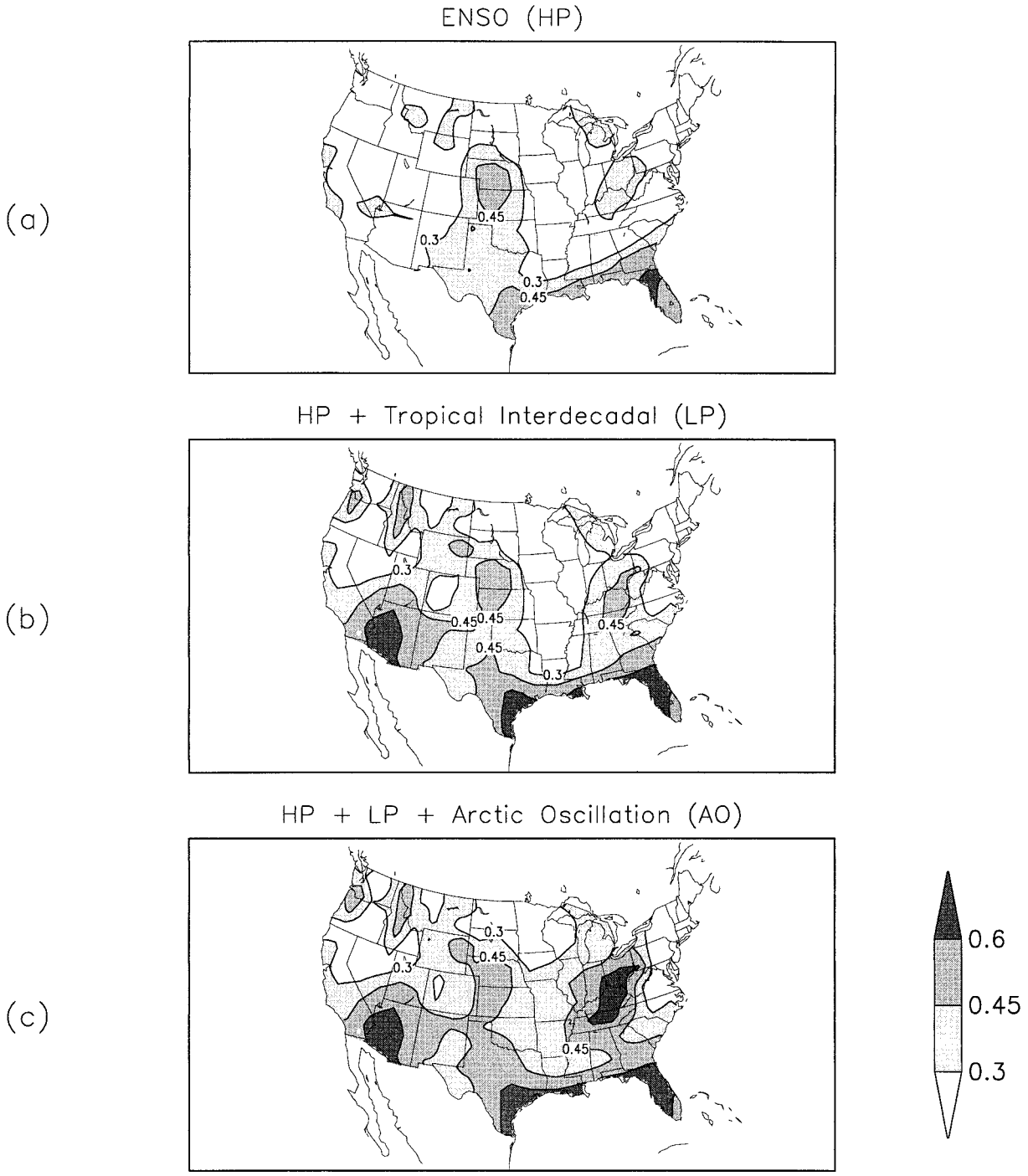


FIG. 11. The 36-yr (1958–93) correlation between time series of JFM observed and JFM reconstructed U.S. precipitation. The reconstructed time series are obtained by regressing the observed precipitation onto (a) the HP index, (b) the HP and LP indices, and (c) the HP, LP, and AO indices. The critical value of the correlation coefficient (significant at the 95% level) is 0.32.

zonally symmetric or ''annular'' structures, with geopotential height perturbations of opposing sign in the polar cap region and the surrounding ring near 45° latitude. These modes were interpreted as the surface signature of fluctuations in the strength of the polar vortex. During the midwinter ''active season'' the NH mode (i.e., the AO) contains an embedded planetary wave signature that influences the hemispheric circulation as well as surface air temperature and precipitation. In a follow-on study Thompson et al. (2000) documented

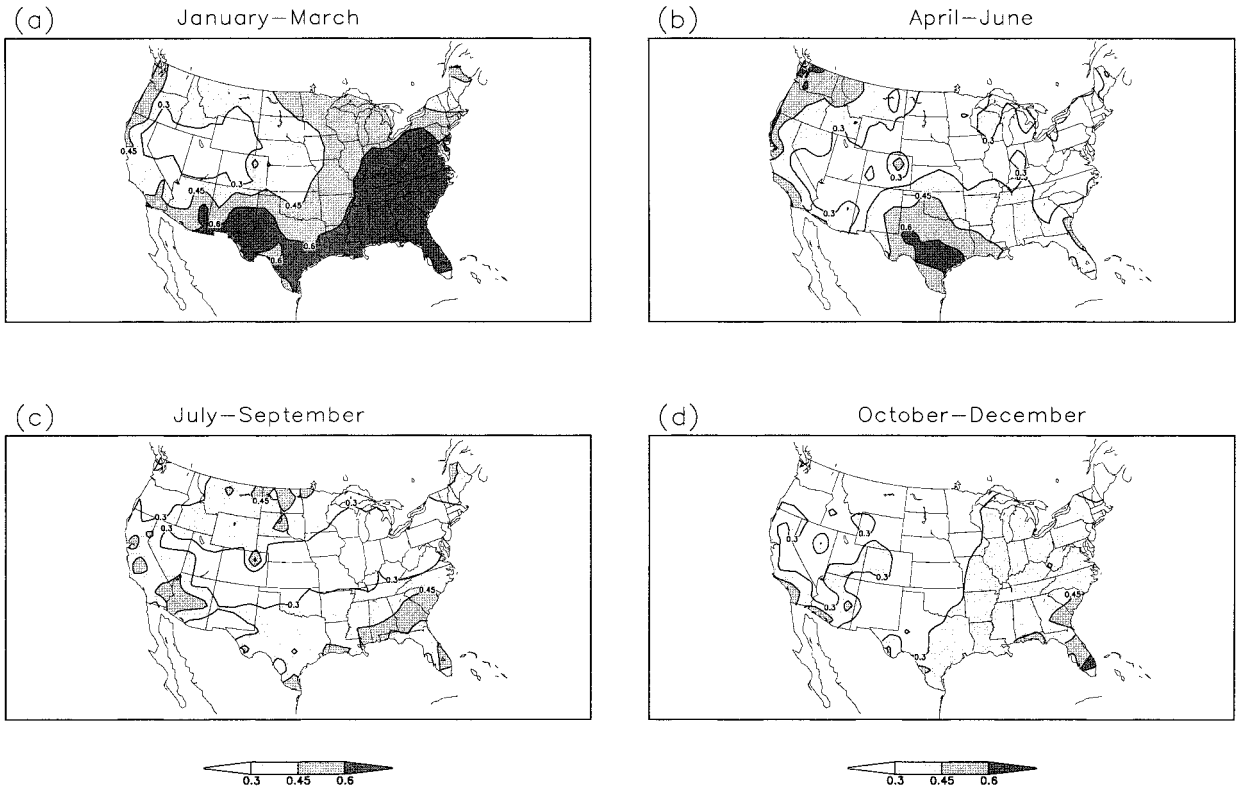


FIG. 12. The 36-yr (1958–93) correlation between time series of observed and reconstructed U.S. surface air temperature for (a) Jan–Mar, (b) Apr–Jun, (c) Jul–Sep, and (d) Oct–Dec. The reconstructed time series are obtained by regressing the observed temperature onto the HP, LP, and AO indices. The critical value of the correlation coefficient (significant at the 95% level) is 0.32.

the striking resemblance between the structure of the annular modes and observed trends over the past 30 yr, including the strengthening of the subpolar westerlies in recent decades. They demonstrated that the observed wintertime warming over Eurasia (Thompson and Wallace 1998), the increasing prevalence of the high index phase of the NAO (Hurrell 1995), and the strengthening of the stratospheric polar night jet (Graf et al. 1995) in recent years all appear to be related to the deepening of the polar vortex. Because the AO encompasses the NAO, this implies that skillful climate predictions in the North Atlantic and over portions of North America (see section 4c) require forecasts of the AO.

The AO index used in this study was kindly provided by D. Thompson and M. Wallace of the University of Washington. Their index was defined on the basis of the standardized leading principal component time series of monthly mean NH sea level pressure (SLP) for all months of the year. The SLP data used to develop the index were obtained from the data support section at NCAR (Trenberth and Paolino 1981).

The AO index is shown in the top panel of Fig. 7. Though not formally orthogonal to the two tropical indices discussed in section 3a, the AO index is essentially uncorrelated with the HP index ($r = -0.10$) and with the LP index ($r = 0.02$), suggesting a good separation of the tropical and extratropical variability.

The spatial signature obtained by regressing the monthly global SST field upon the monthly AO index is shown in the middle panel of Fig. 7. The regression pattern shows localizations in the North Atlantic and the North Pacific, with little amplitude in the Tropics. The North Atlantic pattern appears to be consistent with the NAO. A regression of global SST onto the NAO index of Bell and Halpert (1995) (not shown) produces a similar pattern to that shown in the middle panel of Fig. 7 over the North Atlantic, but very little loading over the North Pacific. We note that the AO index correlates significantly with the NAO index ($r = 0.69$) but is uncorrelated with the Latif and Barnett (1996) North Pacific SST index ($r = -0.01$). A regression of 200-hPa streamfunction onto the AO index (lower panel of Fig. 7) illustrates the association of the AO with the zonal symmetry of the circulation in the NH midlatitudes. We note that the values in the NH midlatitudes are as much as a factor of 4 smaller than those obtained by regressing JFM 200-hPa streamfunction onto JFM values of the AO index (i.e., the active season).

Finally, we note that correlations between annual versions of the LP and AO indices used in this study and

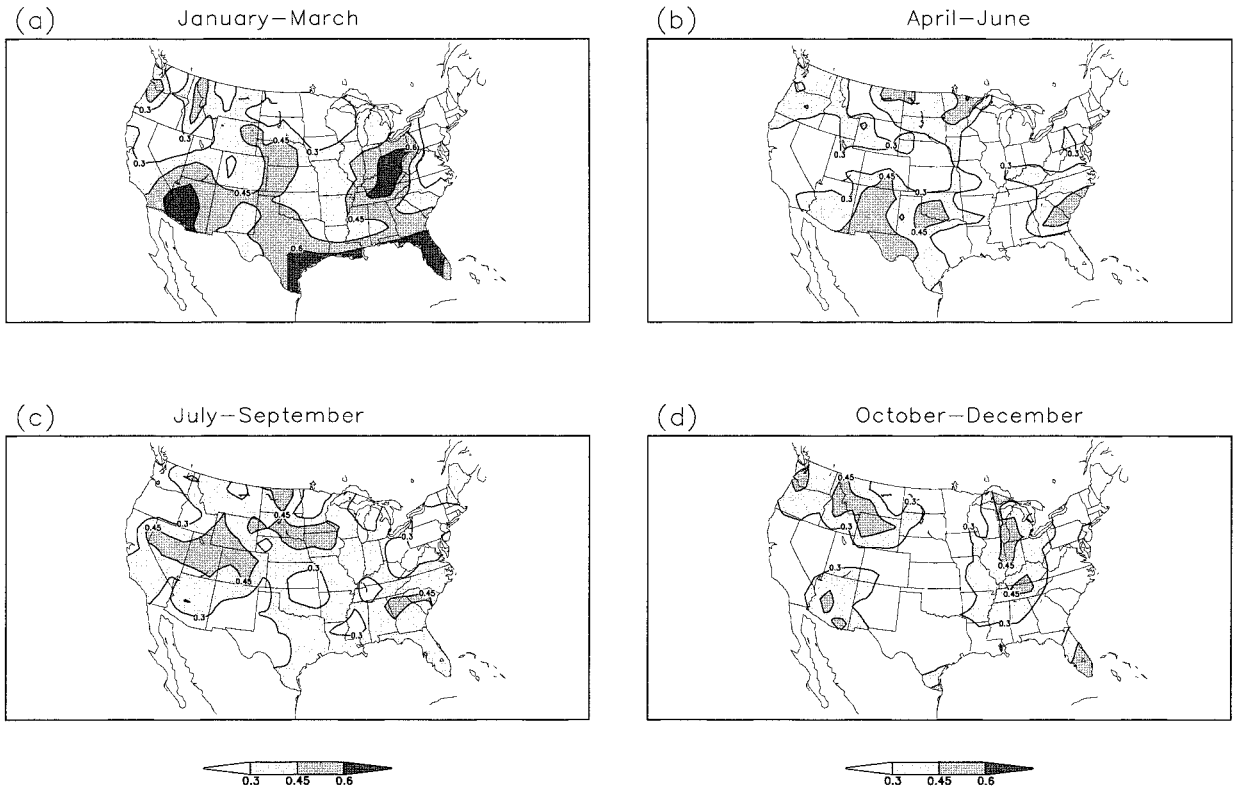


FIG. 13. The 36-yr (1958–93) correlation between time series of observed and reconstructed U.S. precipitation for (a) Jan–Mar, (b) Apr–Jun, (c) Jul–Sep and (d) Oct–Dec. The reconstructed time series are obtained by regressing the observed precipitation onto the HP, LP, and AO indices. The critical value of the correlation coefficient (significant at the 95% level) is 0.32.

the ''trend'' mode of Livezey and Smith (1999) are significant [$r$(LP, trend) = 0.63 and $r$(AO, trend) = 0.38]. It is likely that stronger correlations were not obtained due to differences in the methodology.

## 4. Explained variance

While skillful SST forecasts related to ENSO are routine, forecasts of long-term tropical variability and/or extratropical variability associated with the AO (or NAO) are not. In practice, what might be required are forecasts of appropriate indices, such as the HP, LP, and AO indices, which capture the fundamental variability. But would the skill of a climate forecast system be improved?

A zero-order way to estimate the value added by such forecasts is to compute concurrent correlations between time series of the observations and reconstructed time series, based on linear regressions involving one or more of the indices. Temporal correlation skill benchmarks are established using a cross-validated version of the linear correlation between the observed and reconstructed time series (see section 2). Since forecasts of ENSO are routine, we assume that correlations between observed time series and reconstructed time series, generated by regressing the observations onto the HP index, are a suitable estimate of the state of the art. In the following sections this approach is used to estimate the fraction of the total variance of 1) SST, 2) the upper-tropospheric circulation, and 3) U.S. precipitation and surface air temperature accounted for by our climate decomposition. The focus is on JFM primarily because this is the most active season for the AO (Thompson and Wallace 1998), though its potential importance during the warm season should not be ignored. We will refer to the regressed time series as forecasts, with the implicit understanding that they explain slightly more of the total variance than would be accounted for in true independent forecasting.

### *a. Sea surface temperature*

Correlations between observed and reconstructed time series of JFM SST, in which the HP (Fig. 8a), the HP and LP (Fig. 8b), and the HP, LP, and AO (Fig. 8c) indices are included in the reconstructions, improve considerably with each additional index. The LP (Fig. 8b) increases the explained variance over the central North Pacific and in an arc extending from the Aleutians to the west coast of North America. Other improvements are apparent over the eastern North Atlantic, the central and eastern tropical Pacific (particularly south of the

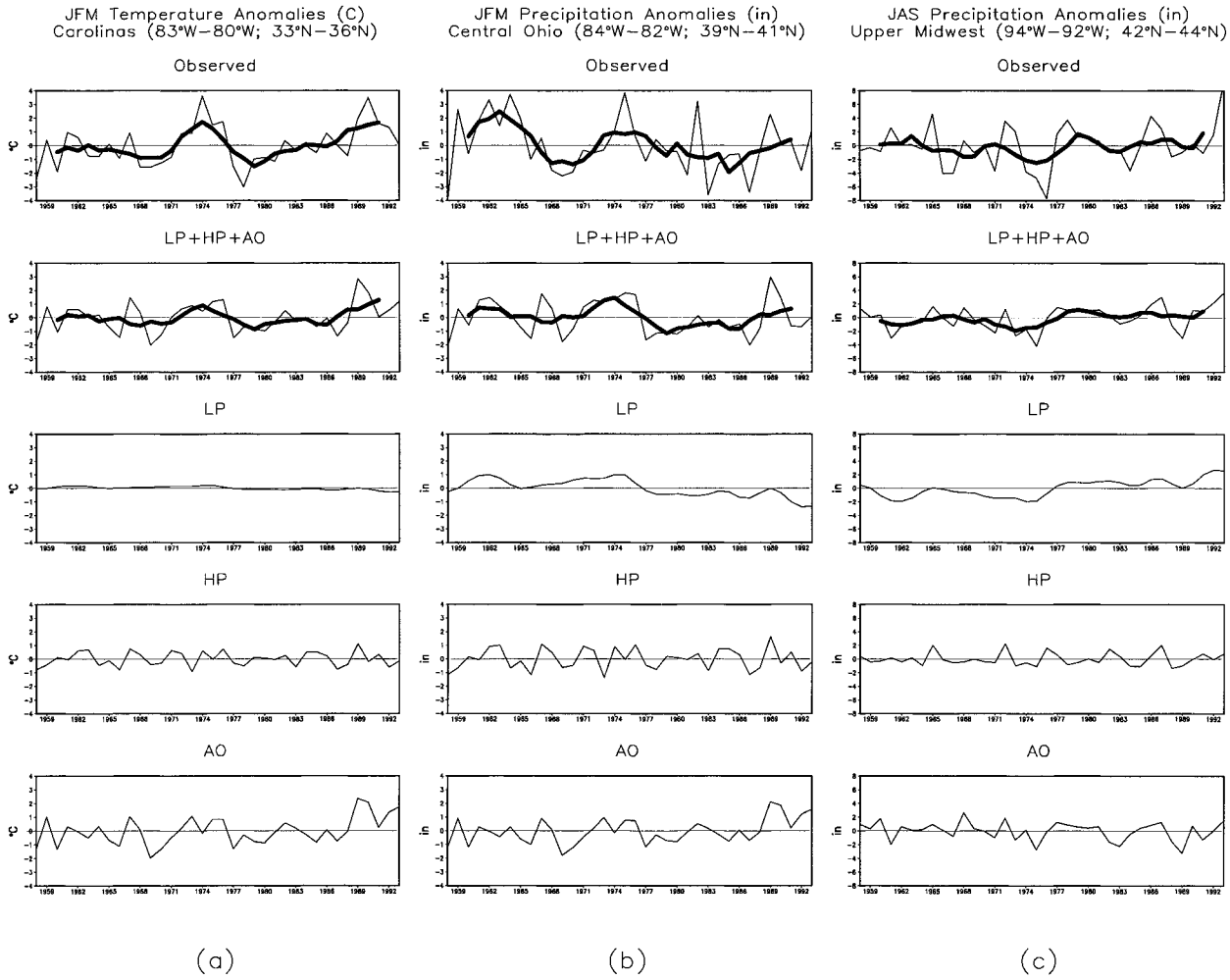


FIG. 14. Time series of (a) JFM temperature anomalies (units: °C) for the Carolinas (33°–36°N, 83°–80°W), (b) JFM precipitation anomalies (in.) for central Ohio (39°–41°N, 84°–82°W), and (c) JAS precipitation anomalies (in.) for the upper Midwest (42°–44°N, 94°–92°W). In each column the observed time series are shown as well as reconstructions of the observed time series onto the LP, HP, and AO indices as indicted. Reconstructed time series, are based on linear regressions involving one or more of the indices. The 5-yr running mean values (thick solid lines) are given in the first two panels of each column. Anomalies are with respect to 1961–90 base period monthly means.

equator), and the eastern Indian Ocean. The AO (Fig. 8c) increases the explained variance further over the North Atlantic. The correlation between time series of observed SST and a reconstruction based on the HP and AO indices (not shown) does not account for the improvements obtained when the HP and LP indices are available (Fig. 8b), except over the North Atlantic where there is an improvement in either case. This is further evidence that the LP and AO indices are nearly independent.

### *b. Upper-tropospheric circulation*

Correlations between observed and reconstructed time series of JFM 200-hPa eddy streamfunction (the term eddy implies that the zonal mean has been removed), in which the HP (Fig. 9a), the HP and LP (Fig. 9b), and the HP, LP, and AO indices (Fig. 9c) are included in the reconstructions, also improve with forecasts of each additional index. The LP (Fig. 9b) increases the explained variance over much of the Tropics and subtropics in each hemisphere, as well as over portions of southeastern Asia and western North America. As was the case for SST (section 4a), the AO (Fig. 9c) increases the explained variance further over much of the North Atlantic and eastern Canada, and to a lesser degree over western Europe and northern Africa.

### *c. U.S. precipitation and surface air temperature*

Correlations between observed and reconstructed time series of JFM surface air temperature over the United States, in which the HP (Fig. 10a), the HP and LP (Fig. 10b), and the HP, LP, and AO (Fig. 10c) indices are included, exhibit regional increases in the explained variance with each additional index. When forecasts of

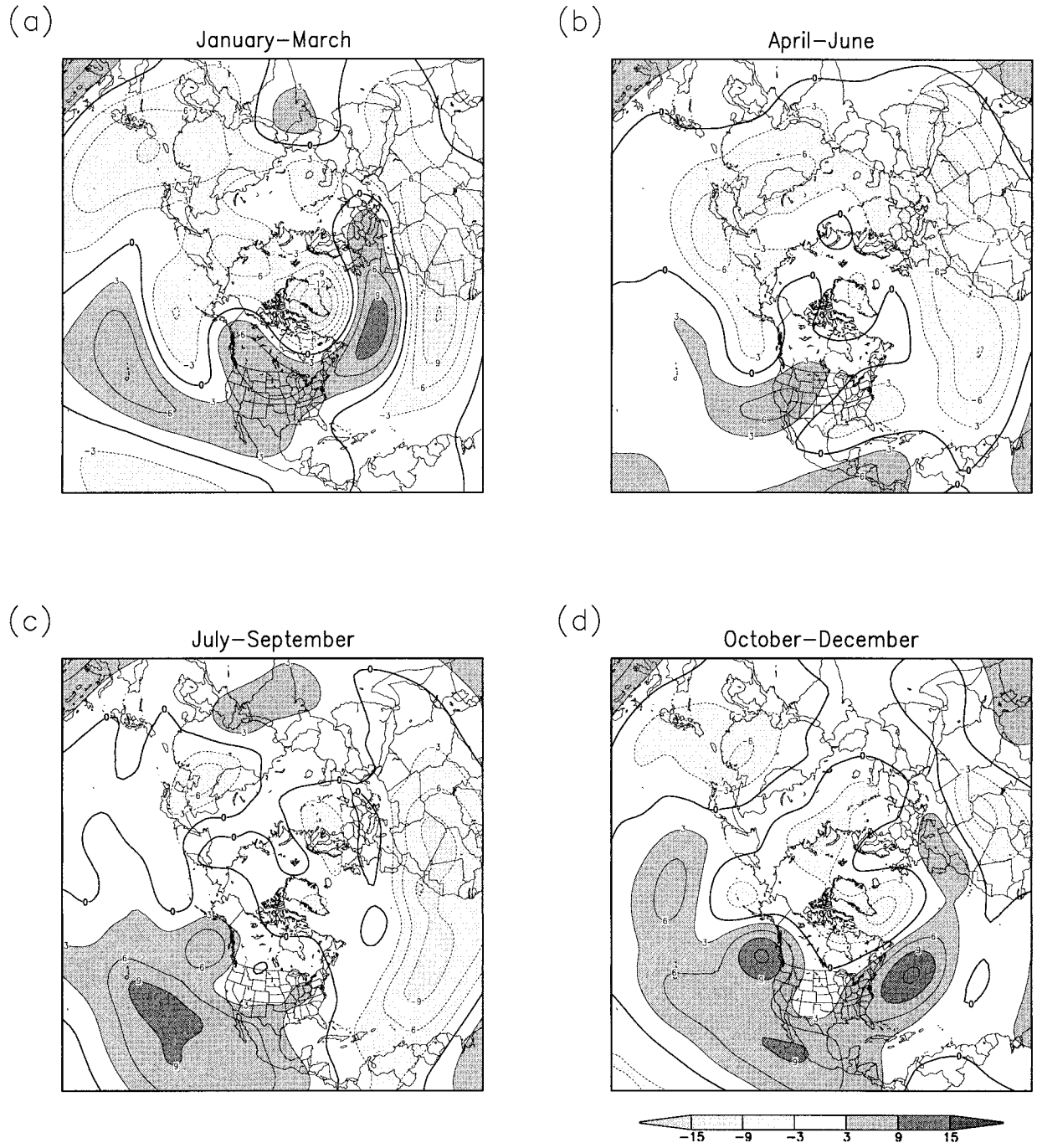


FIG. 15. The 30-yr (1964–93) total linear trends in 200-hPa streamfunction [$10^6$ m$^2$ s$^{-1}$ 30 yr$^{-1}$] for (a) JFM, (b) AMJ, (c) JAS, and (d) OND. The contour interval is $3 \times 10^6$ m$^2$ s$^{-1}$ and the zero contour has been darkened. Dark (light) shading denotes values greater than $+3 \times 10^6$ m$^2$ s$^{-1}$ (less than $-3 \times 10^6$ m$^2$ s$^{-1}$).

the HP and LP indexes are available (Fig. 10b), the explained variance increases over the southwestern United States and to some extent over the northwestern United States. A reconstruction based on all three indexes (Fig. 10c) increases the explained variance considerably over the eastern United States, particularly in the Ohio Valley and the southeast, where correlations exceed 0.7 over the Carolinas. Somewhat surprisingly, a similar calculation with JFM precipitation (Fig. 11) produces comparable increases in the explained variance in the Ohio Valley and along the Gulf coast.

Correlations between observed and reconstructed

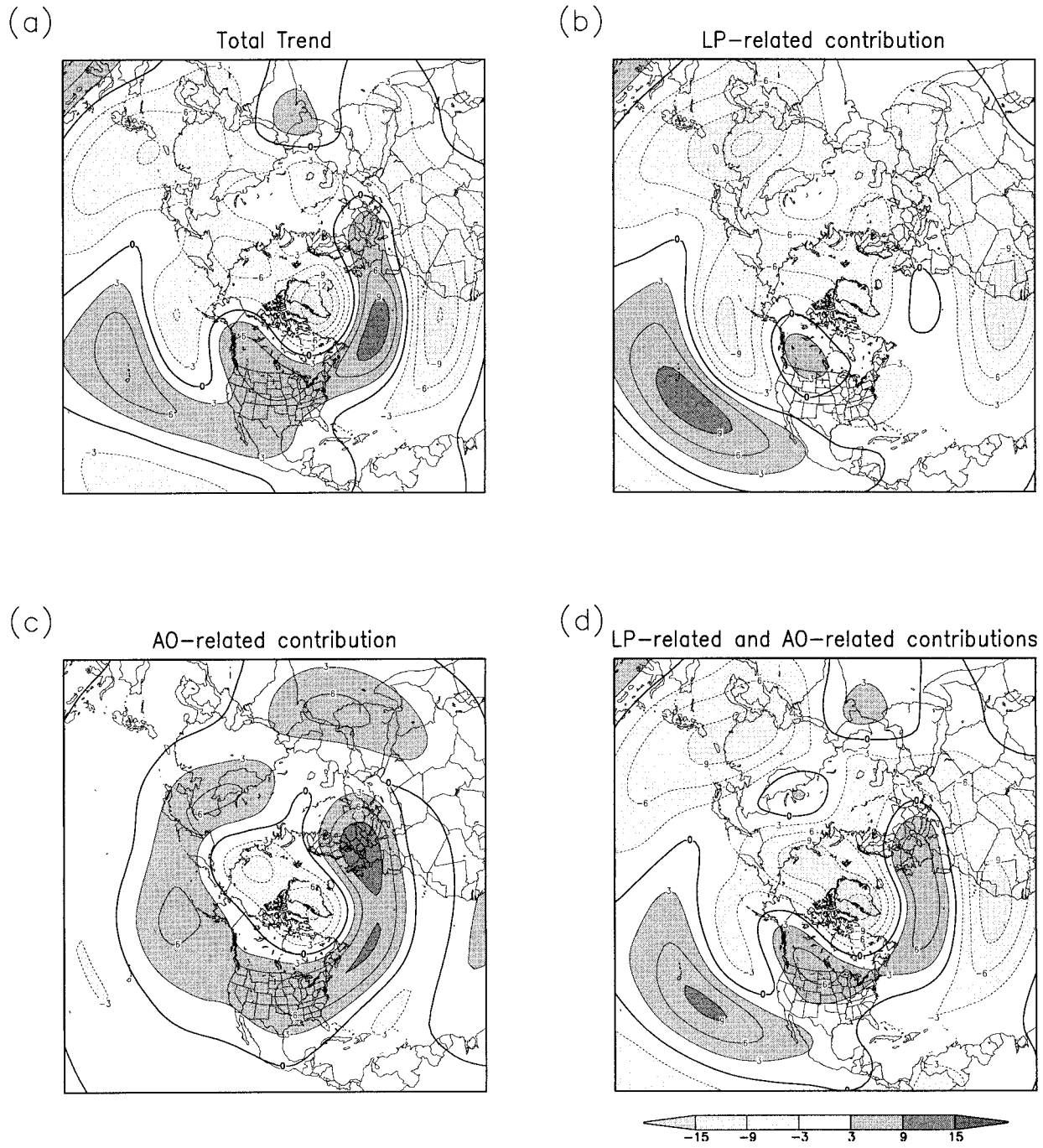


FIG. 16. The 30-yr (1964–93) linear JFM trends in 200-hPa streamfunction [$10^6$ m$^2$ s$^{-1}$ 30-yr$^{-1}$]. (a) The total trend; (b)–(d) the LP-related, AO-related, and LP- and AO-related contributions to the total trend, respectively. The contour interval is $3 \times 10^6$ m$^2$ s$^{-1}$ and the zero contour has been darkened. Dark (light) shading denotes values greater than $+3 \times 10^6$ m$^2$ s$^{-1}$ (less than $-3 \times 10^6$ m$^2$ s$^{-1}$).

time series of United States surface air temperature and precipitation for each season of the year are shown in Figs. 12 and 13, respectively; in each case the reconstructions are based on all three indexes. Notably, the LP-related and AO-related contributions to the seasonal predictability of summer precipitation (Fig. 13c) are significant, particularly in the upper Midwest and intermountain west, suggesting a focus for studies of warm season precipitation prediction.

In order to determine how each mode contributes to the explained variance, it is useful to examine time series of seasonal precipitation and surface air temperature anomalies for selected regions over the United States. For example, time series of observed and reconstructed

TABLE 2. The 30-yr (1964–93) linear trends in U.S. precipitation (expressed as percent departure from the seasonal climatology per 30 yr) and the LP-related and AO-related contributions to the total trend. Estimates are obtained using the methodology outlined in section 2.

| Season | Total trend | LP contribution | AO contribution |
|---|---|---|---|
| JFM | +17 | +14 | +3 |
| AMJ | +6 | +7 | −1 |
| JAS | +7 | +6 | +1 |
| OND | +7 | +2 | +5 |
| Annual | +9 | +7 | +2 |

TABLE 3. The 30-yr (1964–93) linear trends in U.S. surface air temperature (expressed as °C per 36 yr) and the LP-related and AO-related contributions to the total trend. Estimates are obtained using the methodology outlined in section 2.

| Season | Total trend | LP contribution | AO contribution |
|---|---|---|---|
| JFM | +1.1 | +0.5 | +0.6 |
| AMJ | +0.6 | +0.5 | 0.0 |
| JAS | 0.2 | +0.1 | +0.1 |
| OND | −0.3 | −0.2 | −0.1 |
| Annual | +0.4 | +0.2 | +0.2 |

JFM temperature anomalies for the Carolinas (Fig. 14a) illustrate the degree to which interannual variability is captured by our reconstruction. In particular, the HP-related and especially the AO-related contributions to the observed variability are large, but LP-related contributions are negligible. By contrast, JFM temperature anomalies in the northern plains are dominated by LP-related contributions (not shown).

JFM precipitation in central Ohio (Fig. 14b) has exhibited a drying trend, as indicated by LP-related contributions, but HP-related and AO-related contributions account for interannual swings superimposed on this trend. LP-related and AO-related contributions also account for the gradual increase in JFM precipitation along the Gulf coast (not shown), with HP-related contributions accounting for many of the extreme events. Time series of JAS precipitation in the upper Midwest (Fig. 14c) show a slight trend toward wetter conditions, as exhibited by LP-related contributions. Note in particular that the 1993 flood appears to be due to multiple causes, not a single cause (i.e., ENSO). The examples in Fig. 14 illustrate how our climate decomposition might be used to identify potential causal mechanisms that contribute to climate anomalies, such as floods and droughts.

## 5. Contributions to recent trends

In this section we focus on LP-related and AO-related contributions to recent (1964–93) trends. We emphasize

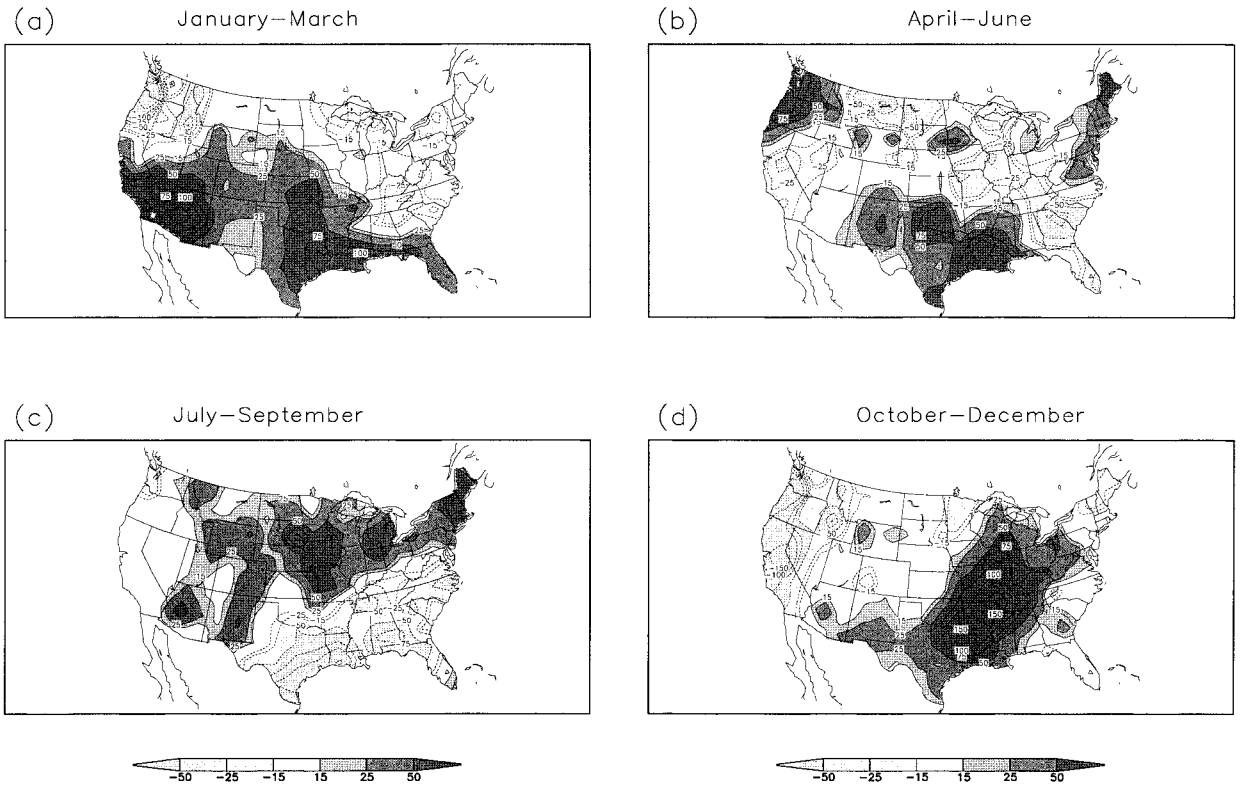


FIG. 17. The 30-yr (1964–93) total linear trends in U.S. precipitation [mm (30 yr)$^{-1}$] for (a) JFM, (b) AMJ, (c) JAS, and (d) OND. The contour interval is 25 mm (to which the +15 mm and −15 mm intervals have been added). The zero contour has been omitted for clarity. Dark (light) shading denotes values greater than +15 mm (less than −15 mm).

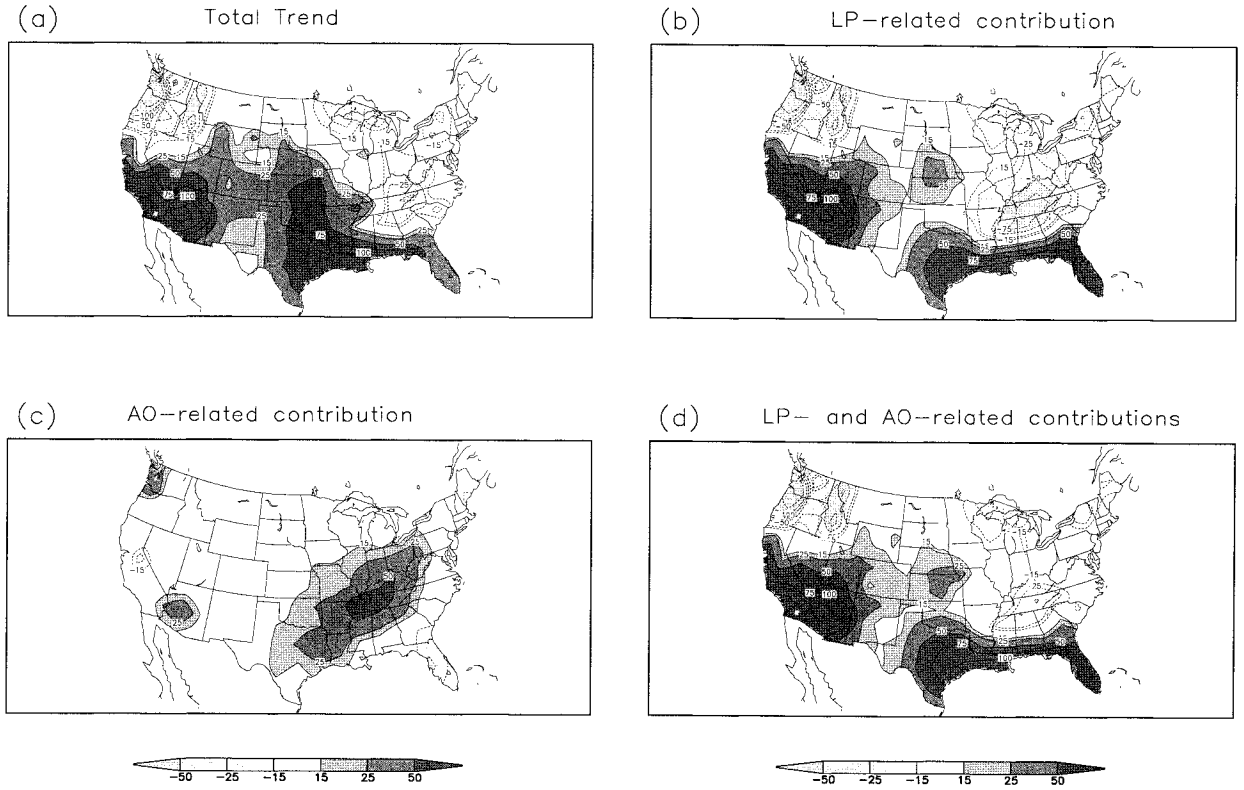


FIG. 18. The 30-yr (1964–93) linear JFM trends in U.S. precipitation [mm (30 yr)$^{-1}$]. (a) The total trend; (b)–(d) the LP-related, AO-related, and LP- and AO-related contributions to the total trend, respectively. The contour interval is 25 mm (to which the +15 mm and −15 mm intervals have been added). The zero contour has been omitted for clarity. Dark (light) shading denotes values greater than +15 mm (less than −15 mm).

NH winter (JFM) since this is the time of year when fluctuations in the AO are important (Thompson and Wallace 2000) as well as when HP (ENSO) effects are most prominent. We will investigate the signature of each index in the upper-tropospheric circulation and in U.S. precipitation and surface air temperature. Results from other seasons are also given.

### *a. Linear trends in the indices*

Linear 30-yr (1964–93) annual mean total trends in the LP, HP, and AO indexes are +2.5, +0.2, and +1.9, in units of std dev (30 yr)$^{-1}$ (1964–93). Positive trends are evident in all three indexes, but significant trends (estimated using the *t*-statistic applied to the linear correlation coefficient between the time axis and the index values) are found only in the LP and AO indexes.

The seasonality of the trend in the LP index was examined by computing seasonal EOFs (using a 7-yr running mean on the seasonal mean data). We found that there is negligible seasonality of the trend in the LP index. On the other hand, Thompson et al. (2000) showed that there is considerable seasonality of the trend in the AO index (e.g., see their Table 1), with the largest trends during the active season (JFM). While the HP index does not exhibit a significant trend in any season, there is considerable seasonal variability in its strength that must be accounted for.

### *b. Upper-tropospheric circulation*

Over the last few decades there have been large and significant trends in the NH upper-tropospheric circulation. Charts showing the total trend in 200-hPa streamfunction for each season during the 30-yr period (1964–93) are given in Fig. 15. The largest trends during JFM (Fig. 15a) are over the North Atlantic, where the circulation features are consistent with a poleward shift of the North Atlantic jetstream. A latitude–pressure cross section of the 30-yr trend in the JFM zonal mean zonal wind (not shown) is characterized by a strengthening of the westerly flow poleward of 45°N from the surface to 100 hPa and a weakening of the westerlies in the troposphere equatorward of 45°N. JFM trends in the 200-hPa streamfunction over the United States are dominated by anticyclonic flow, consistent with strong warming along the northern tier of states (see Fig. 19a below). The summer (JAS) trend (Fig. 15c) shows an increase in the intensity of the tropical upper-tropospheric trough over the North Atlantic basin, consistent with increased westerly shear and suppressed Atlantic hurricane activity in the more recent period (at least through 1993).

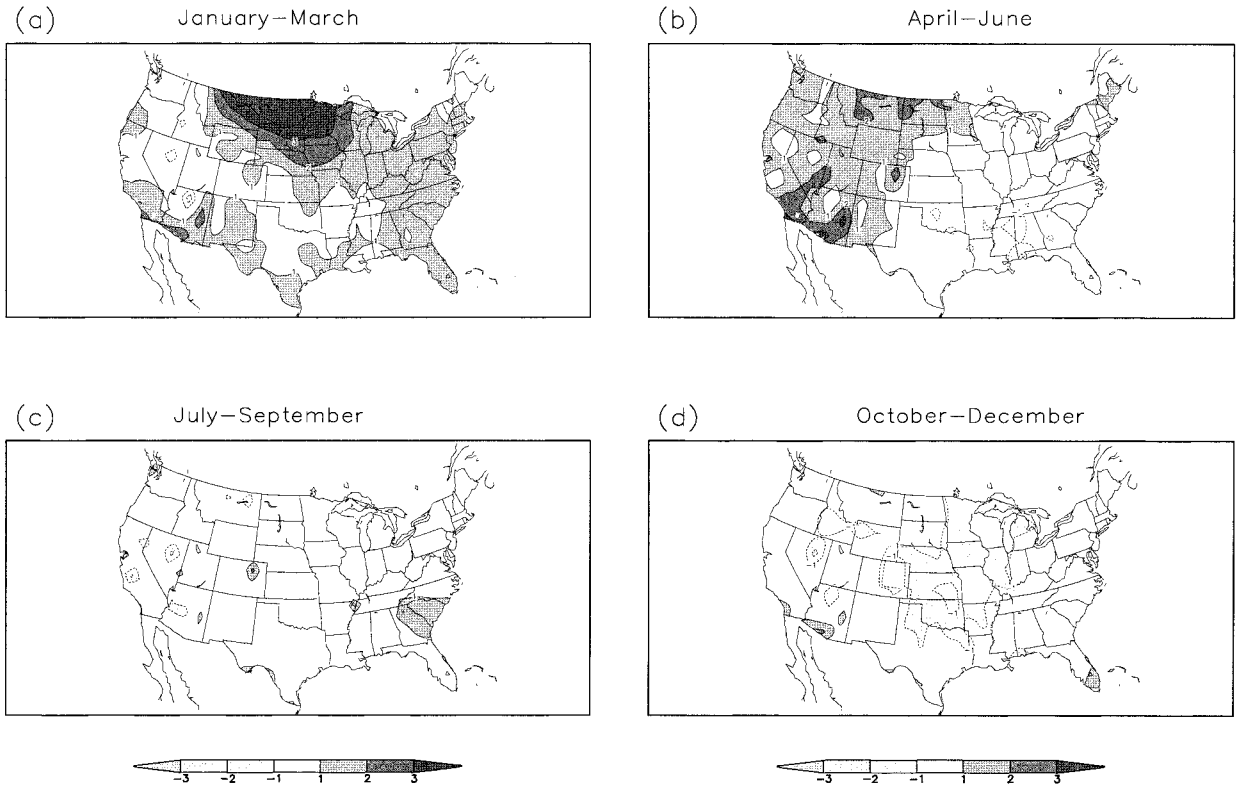


FIG. 19. The 30-yr (1964–93) total linear trends in U.S. surface air temperature [°C (30 yr)$^{-1}$] for (a) JFM, (b) AMJ, (c) JAS, and (d) OND. The contour interval is 1°C. The zero contour has been omitted for clarity. Dark (light) shading denotes values greater than +1°C (less than −1°C).

The slight increase in the intensity of the upper-tropospheric anticyclonic circulation over southwestern North America appears to be consistent with increasing precipitation in this region (see Fig. 17c below). An examination of the monthly data is necessary to determine whether this is due to increased monsoon precipitation and/or to increased tropical storm activity in this region during the summer. During autumn (OND), the upper-tropospheric anticyclone over the western North Atlantic has strengthened, consistent with increased surface cyclogenesis (not shown) and precipitation in the south-central United States (see Fig. 17d below).

An examination of LP-related and AO-related contributions to the total trend in 200-hPa streamfunction during JFM (Fig. 16) indicates that neither mode dominates the total trend. Over the North Pacific the total trend is largely due to LP-related contributions, which are generally in the opposite sense to the AO-related contributions. The pattern over the North Pacific shows a pronounced split in the flow consistent with the high index polarity of the PNA pattern. Zhang et al. (1997) and Trenberth and Hurrell (1994) attributed the features over the North Pacific/western North America to ''ENSO-like'' interdecadal variability and the 1976–77 ''regime shift.'' Over the northern North Atlantic the total trend is dominated by AO-related contributions that exhibit considerable zonal symmetry. Over southeastern portions of the North Atlantic the LP-related contributions (Fig. 16b) dominate the total trend. The structural similarity between the total trend and the corresponding combined signature of the LP-related and AO-related contributions (Fig. 16d) is striking, though the amplitudes of the reconstructed field are generally only moderate.

### *c. U.S. precipitation and surface air temperature*

Over the last few decades there have been large and significant trends in U.S. precipitation and surface air temperature. Seasonal precipitation and surface air temperature trends over the conterminous United States for the 30-yr period (1964–93) are given in Tables 2 and 3, respectively. The LP-related and AO-related contributions to the total trends (computed using the procedure outlined in section 2) are also given.

Table 2 shows that total trends in precipitation for the conterminous United States are positive for each season of the year. The LP-related and AO-related contributions account for virtually all of the observed trend. The table also shows that total trends are dominated by LP-related contributions in all seasons of the year except OND, when AO-related contributions dominate the total trend.

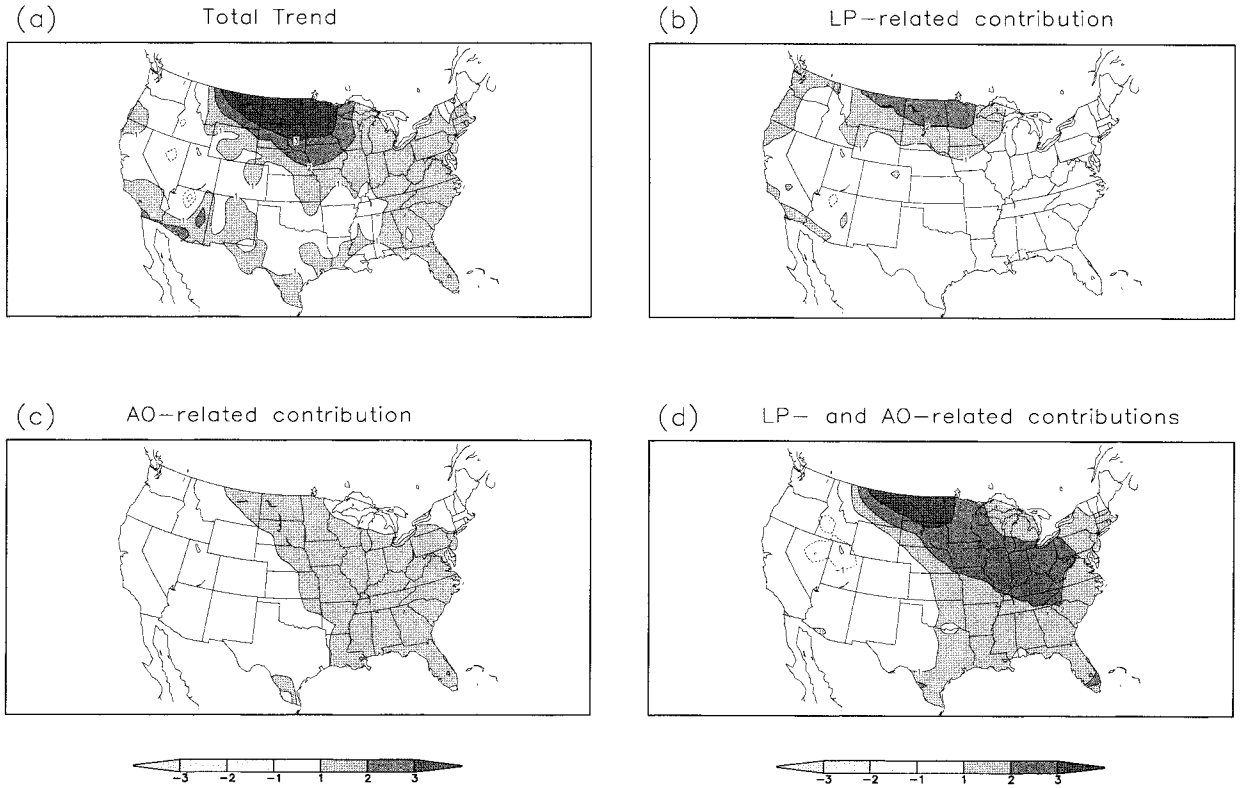


FIG. 20. The 30-yr (1964–93) linear JFM trends in U.S. surface air temperature [°C (30 yr)$^{-1}$] (a) The total trend; (b)–(d) the LP-related, AO-related, and LP- and AO-related contributions to the total trend, respectively. The contour interval is 1°C. The zero contour has been omitted for clarity. Dark (light) shading denotes values greater than +1°C (less than −1°C).

Charts showing the total observed precipitation trend for each season are given in Fig. 17. The largest regional trends in JFM precipitation include decreased precipitation over the Pacific Northwest and increased precipitation in the southwest and southeast (Fig. 17a). The total trend pattern resembles a typical wintertime El Niño precipitation anomaly pattern. The LP-related contributions (Fig. 18b) account for much of the total observed trend at most locations. One exception is in the Ohio and Tennessee Valleys, where AO-related contributions are large and positive (Fig. 18c) and generally in the opposite sense to LP-related contributions.

The spring (AMJ) trend in precipitation (Table 2) is mainly due to increases along the Gulf coast (particularly Louisiana) and in the Pacific Northwest (Fig. 17b). A spring drying trend has occurred over Georgia and the Carolinas. The summer season (Fig. 17c) shows a surprisingly coherent large-scale pattern, with increasing precipitation in a band extending from the southwestern United States to New England and decreasing precipitation along the Gulf coast from Texas to the Carolinas. Increasing precipitation in the southwest appears to be related to enhanced monsoon activity, particularly during the 1980s (e.g., Higgins et al. 1999; Higgins and Shi 2000) while that in the upper Midwest and New England is related to enhanced activity along the polar front. Autumn increases in precipitation are quite large over the south-central United States (Fig. 17d), where precipitation has increased by as much as 150 mm per season over the last 30 yr at some locations. Much of this trend can be attributed to the AO (not shown), though the LP also contributes. These trends are consistent with changes in the large-scale circulation (e.g., Fig. 15d). Trends in surface air temperature for the conterminous United States are also generally positive, except during autumn when there has been a slight cooling trend (Table 3). Again we find that LP-related and AO-related contributions account for virtually all of the observed trend.

Charts showing recent (1964–93) trends in the observed surface air temperature for each season are given in Fig. 19. In each case these trends are consistent with those in the upper-tropospheric circulation (Fig. 15). Trends during JFM (Fig. 19a) are dominated by strong warming along the northern tier of states, with maximum values larger than 4°C per 30 yr over the far northern plains. The majority of the total trend over this region can be attributed to LP-related contributions, but the AO also participates (Fig. 20). Over the eastern United States the more gradual warming trend appears to be due to AO-related contributions (Fig. 20c). Correlations between JFM surface air temperature and the AO are

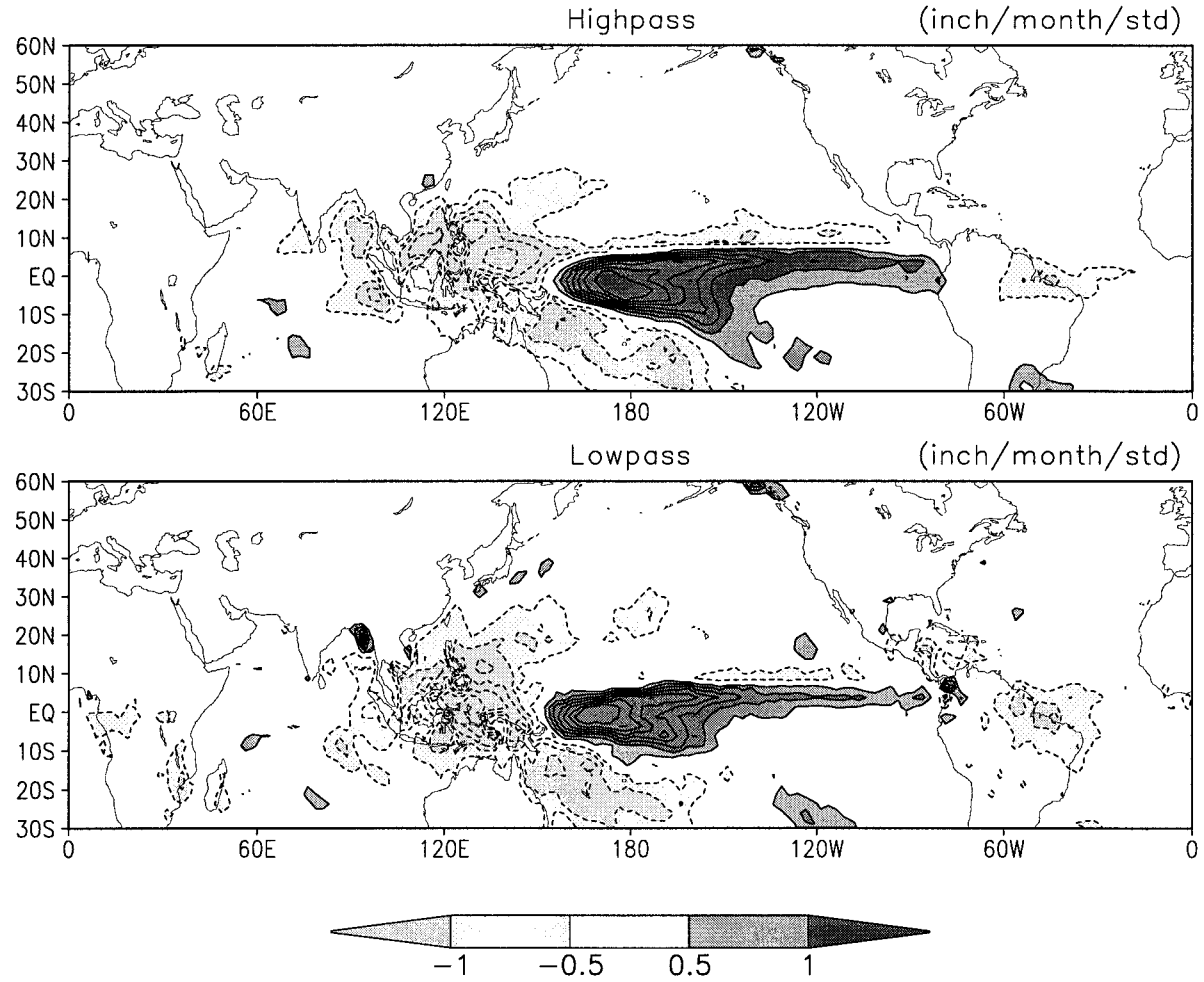


FIG. 21. Spatial patterns generated by regressing monthly global precipitation upon the HP and LP indices shown in the top panels of Fig. 2. Contour interval is 0.5 in. (std dev)$^{-1}$ of the expansion coefficient time series. Negative contours are dashed and the zero contour is thickened. Positive (negative) values greater than 0.5 in. (std dev)$^{-1}$ [less than $-0.5$ in. (std)$^{-1}$] are shaded dark (light). Data source is the CPC merged analysis of precipitation (Xie and Arkin 1996, 1998).

highly significant over the eastern third of the United States (not shown). JFM surface air temperature over the northern plains correlates significantly with JFM values of all three indices (i.e., LP, HP, and AO), suggesting that the warming in this region is not simply a manifestation of global change. The winter warming trend over the southwestern United States discussed by Livezey and Smith (1999; see their Fig. 3) is considerably weaker here, possibly because our anomalies carry the physical units while their anomalies were standardized.

Increases in autumn precipitation over the interior eastern United States during the last 30 yr (Fig. 17d) have been accompanied by cooler surface air temperatures over the north-central United States (Fig. 19d). This trend is consistent with an enhanced upper-tropospheric trough over the northern plains (Fig. 15d) and increased lower-tropospheric northwesterly flow into the northern and central United States (not shown). Over the conterminous United States the temperature trends during the spring (Fig. 19b) and summer (Fig. 19c) appear to be small. However, it is important to recognize that the standard deviation of the temperature field is much smaller in the warm half of the year (e.g., see Fig. 8 of Barnston 1996).

## 6. Discussion

Recent advances in climate-observing and climate-forecast systems prior to the 1997–98 El Niño resulted in unprecedented skill in operational seasonal temperature and precipitation forecasts, such as those produced by the CPC and the International Research Institute for Climate Prediction. Improvements in the supporting link between forecasts and their practical application helped mitigate climate-related impacts in affected sectors (agriculture, water resource management, disaster preparedness, human health, etc.). During this event, fore-

casts based on statistics and based on GCMs were roughly equally skillful (e.g., Barnston et al. 1999).

While a number of GCMs are capable of producing the average response of the atmosphere to changes in the tropical Pacific SSTs associated with extreme ENSO events, such as the 1997–98 El Niño, they are much less successful in reproducing the atmospheric response to typical ENSO SSTs and to less typical SST distributions. Clearly, there is a need to focus on the latter if we are to extend predictability for seasonal to interannual variability.

In this study we presented evidence that a significant portion of the skill of climate forecast models will arise from an ability to forecast the temporal and spatial variability of decade-scale shifts in tropical precipitation and the associated teleconnection patterns into midlatitudes. In particular, it was shown that systematic shifts in tropical convection on decadal timescales contribute significantly to U.S. and global climate variability, particularly trends. Thus, the next significant breakthrough in climate forecasts will come from developing the capability to forecast these more subtle variations in precipitation in the Tropics. Additional increases in predictability are linked to the ability to forecast the NAO aspect of the AO in the North Atlantic sector. Consistent with previous studies, we find that the largest and most significant AO-related contributions over the United States are during the cold season (October–March).

Thus, in practical terms we envision forecasts of at least three indices, such as the HP, LP, and AO indices. It is important to recognize that the skill estimates presented here are from a particular model that only includes these selected influences. There are many other possible influences, such as additional circulation modes, soil moisture, persistence, etc., that may provide skill in various regions and for certain seasons. These other possibilities must be recognized and incorporated. Based on the work of Livezey and Smith (1999), we are undertaking additional work aimed at understanding the relationship between their northern extratropical mode and the AO; in particular, it may be necessary to develop high-pass and low-pass versions of the AO index.

Our rationale for using precipitation rather than SST to represent variability in the Tropics is the more direct physical linkage between fluctuations in the atmospheric circulation and fluctuations in tropical precipitation. Of course, this advantage must be weighed against potential disadvantages due to spatial gaps in the station network. Regressions of the Climate Prediction Center merged precipitation analysis (Xie and Arkin 1996, 1998) onto the HP and LP indices (Fig. 21) produce patterns that incorporate all of the features shown in Fig. 2 (with minor differences in amplitude), indicating that spatial gaps in the island network are probably not a major disadvantage.

It is hoped that these results will provide some direction for the future development of climate forecast systems. Programmatic efforts aimed at improving seasonal prediction in climate forecast systems must devote considerable resources to the two critical ''source'' phenomena identified and discussed here in order to achieve the desired increase in skill.

*Acknowledgments.* The authors are indebted to Vernon Kousky, Masao Kanamitsu, and Robert Livezey for careful reviews of a preliminary draft of this work. We gratefully acknowledge David Thompson and Mike Wallace for the AO index used in this study. The authors also wish to thank Tom Smith and Dick Reynolds for the sea surface temperature data, John Janowiak and Gerry Bell for the U.S. surface air temperature data, Yuxiang He for the Pacific basin monthly precipitation data, Ping-Ping Xie for the global merged precipitation analysis, and the NCEP/NCAR Reanalysis Team for the reanalysis data. This work was partially supported by the NOAA Office of Global Programs under the Pan American Climate Studies (PACS) Project 8R1A69WH and the GEWEX Continental-Scale International Project (GCIP) 8R1DA118.

## REFERENCES

Barnston, A. G., 1996: Time-scales of the variability of the atmosphere. *Int. J. Climatol.*, **16,** 499–535.

——, and H. M. van den Dool, 1993: A degeneracy in cross-validated skill in regression-based forecasts. *J. Climate,* **6,** 963–977.

——, M. H. Glantz, and Y. He, 1999: Predictive skill of statistical and dynamical climate models in SST forecasts during the 1997–98 El Niño episode and the 1998 La Niña onset. *Bull. Amer. Meteor. Soc.,* **80,** 217–243.

Bell, G. D., and M. S. Halpert, 1995: *Interseasonal and interannual variability: 1986–1993.* NOAA Atlas 12, 256 pp.

Deser, C., and M. L. Blackmon, 1995: On the relationship between tropical and North Pacific sea surface temperature variations. *J. Climate,* **8,** 1677–1680.

Douglas, A. V., D. R. Cayan, and J. Namias, 1982: Large-scale changes in North Pacific and North American weather patterns in recent decades. *Mon. Wea. Rev.,* **110,** 1851–1862.

Gibson, J. K., P. Kallberg, S. Uppala. A. Hernandez, A. Nomura, and E. Serrano, 1997: *ERA Description.* ERA Project Rep. Series, No. 1, ECMWF, 72 pp.

Graf, H.-F., J. Perlwitz, I. Kirchner, and I. Schult, 1995: Recent northern winter climate trends, ozone changes and increased greenhouse forcing. *Contrib. Atmos. Phys.,* **68,** 233–248.

He, Y., A. Barnston, and A. Hilton, 1998: *A Precipitation Climatology for Stations in the Tropical Pacific Basin: Effects of ENSO.* NCEP/Climate Prediction Center Atlas 5, 280 pp.

Higgins, R. W., and W. Shi, 2000: Dominant factors responsible for interannual variability of the summer monsoon in the southwestern United States. *J. Climate,* **13,** 759–776.

——, J. E. Janowiak, and Y. Yao, 1996: *A Gridded Hourly Precipitation Data Base for the United States (1963–1993).* NCEP/Climate Prediction Center Atlas 1, 47 pp.

——, Y. Chen, and A. V. Douglas, 1999: Interannual variability of the North American warm season precipitation regime. *J. Climate,* **12,** 653–680.

Hurrell, J. W., 1995: Decadal trends in the North Atlantic Oscillation region temperatures and precipitation. *Science,* **269,** 676–679.

——, and H. van Loon, 1997: Decadal variations in climate associated with the North Atlantic Oscillation. *Climatic Change,* **36,** 301–326.

Janowiak, J. E., G. D. Bell, and M. Chelliah, 1999: *A Gridded Data*

*Base of Daily Temperature Maxima and Minima for the Conterminous United States: 1948–1993*. NCEP/Climate Prediction Center Atlas 6, 50 pp.

Kalnay, E., and Coauthors, 1996: The NCEP/NCAR 40-Year Reanalysis Project. *Bull. Amer. Meteor. Soc.,* **77,** 437–471.

Latif, M., and T. P. Barnett, 1996: Decadal climate variability over the North Pacific and North America: Dynamics and predictability. *J. Climate,* **9,** 2407–2423.

——, R. Kleeman, and C. Eckert, 1997: Greenhouse warming, decadal variability, or El Niño? An attempt to understand the anomalous 1990s. *J. Climate,* **10,** 2221–2239.

Livezey, R. E., and T. M. Smith, 1999: Covariability of aspects of North American climate with global sea surface temperatures on interannual to interdecadal timescales. *J. Climate,* **12,** 289–302.

Parker, D. E., and C. K. Folland, 1991: Worldwide surface air temperature trends since the mid-19th century. *Greenhouse-Gas Induced Climate Change: A Critical Appraisal of Simulations and Observations,* M. E. Schlesinger, Ed., Elsevier, 173–193.

Peng, P., A. Kumar, A. G. Barnston, and L. Goddard, 2000: Simulation skills of the SST-forced global climate variability of the NCEP MRF9 and the Scripps–MPI ECHAM3 Models. *J. Climate,* **13,** 3657–3679.

Rasmusson, E. M., and T. H. Carpenter, 1982: Variations in tropical sea surface temperature and surface wind fields associated with the Southern Oscillation/El Niño. *Mon. Wea. Rev.,* **110,** 354–384.

Reynolds, R. W., and T. M. Smith, 1995: A high resolution global sea surface temperature climatology. *J. Climate,* **8,** 1571–1583.

Ropelewski, C. F., J. E. Janowiak, and M. S. Halpert, 1985: The analysis and display of real time surface climate data. *Mon. Wea. Rev.,* **113,** 1101–1106.

Smith, T. M., R. W. Reynolds, R. E. Livezey, and D. C. Stokes, 1996: Reconstruction of historical sea surface temperatures using empiracle orthogonal functions. *J. Climate,* **9,** 1403–1420.

Thompson, D. W. J., and J. M. Wallace, 1998: The arctic oscillation signature in the wintertime geopotential height and temperature fields. *Geophys. Res. Lett.,* **25,** 1297–1300.

——, and ——, 2000. Annular modes in the extratropical circulation. Part I: Month-to-month variability. *J. Climate,* **13,** 1000–1016.

——, ——, and G. C. Hegerl, 2000: Annular modes in the extratropical circulation. Part II: Trends. *J. Climate,* **13,** 1018–1036.

Trenberth, K. E., and D. A. Paolino, 1981: Characteristic patterns of variability of sea level pressure in the Northern Hemisphere. *Mon. Wea. Rev.,* **109,** 1169–1189.

——, and J. W. Hurrell, 1994: Decadal atmospheric–ocean variations in the Pacific. *Climate Dyn.,* **9,** 303–309.

Wang, B., 1995: Interdecadal changes in El Niño onset in the last four decades. *J. Climate,* **8,** 267–285.

Xie, P., and P. A. Arkin, 1996: Analyses of global monthly precipitation using gauge observations, satellite estimates, and numerical model predictions. *J. Climate,* **9,** 840–858.

——, and ——, 1998: Global monthly precipitation estimates from satellite-observed outgoing longwave radiation. *J. Climate,* **11,** 137–164.

Yukimoto, S., M. Endoh, Y. Kitamura, A. Kitoh, T. Motoi, A. Noda, and T. Tokioka, 1996: Interannual and interdecadal variabilities in the Pacific in an MRI coupled GCM. *Climate Dyn.,* **12,** 667–683.

Zhang, Y., J. M. Wallace, and D. Battisti, 1997: ENSO-like interdecadal variability: 1900–1993. *J. Climate,* **10,** 1004–1020.